

# Polygenic Adaptation: From sweeps to subtle frequency shifts

Ilse Höllinger<sup>1,2</sup>, Pleuni Pennings<sup>3</sup>, and Joachim Hermisson<sup>1</sup>

<sup>1</sup>Mathematics and BioSciences Group, Faculty of Mathematics and Max F. Perutz Laboratories, University of Vienna, Vienna, Austria

<sup>2</sup>Vienna Graduate School of Population Genetics, Vienna, Austria

<sup>3</sup>Department of Biology, San Francisco State University, California, USA

October 23, 2018

**Postal address:**

Joachim Hermisson and Ilse Höllinger  
Faculty of Mathematics, University of Vienna  
Oskar-Morgenstern-Platz 1  
1090 Wien, Austria  
Europe

**Telephone number:**

+43/1/4277 50648 (J. Hermisson)  
+43/1/4277 50771 (I. Höllinger)

**Email-address:**

joachim.hermisson@univie.ac.at (J. Hermisson)  
pennings@sfsu.edu (P. Pennings)  
ilse.hoellinger@univie.ac.at (I. Höllinger)

## Abstract

Evolutionary theory has produced two conflicting paradigms for the adaptation of a polygenic trait. While population genetics views adaptation as a sequence of selective sweeps at single loci underlying the trait, quantitative genetics posits a collective response, where phenotypic adaptation results from subtle allele frequency shifts at many loci. Yet, a synthesis of these views is largely missing and the population genetic factors that favor each scenario are not well understood. Here, we study the architecture of adaptation of a binary polygenic trait (such as resistance) with negative epistasis among the loci of its basis. The genetic structure of this trait allows for a full range of potential architectures of adaptation, ranging from sweeps to small frequency shifts. By combining computer simulations and a newly devised analytical framework based on Yule branching processes, we gain a detailed understanding of the adaptation dynamics for this trait. Our key analytical result is an expression for the joint distribution of mutant alleles at the end of the adaptive phase. This distribution characterizes the polygenic pattern of adaptation at the underlying genotype when phenotypic adaptation has been accomplished. We find that a single compound parameter, the population-scaled background mutation rate  $\Theta_{bg}$ , explains the main differences among these patterns. For a focal locus,  $\Theta_{bg}$  measures the mutation rate at all redundant loci in its genetic background that offer alternative ways for adaptation. For adaptation starting from mutation-selection-drift balance, we observe different patterns in three parameter regions. Adaptation proceeds by sweeps for small  $\Theta_{bg} \lesssim 0.1$ , while small polygenic allele frequency shifts require large  $\Theta_{bg} \gtrsim 100$ . In the large intermediate regime, we observe a heterogeneous pattern of partial sweeps at several interacting loci.

# 1 Author summary

1 It is still an open question how complex traits adapt to new selection pressures.  
2 While population genetics champions the search for selective sweeps, quantitative  
3 genetics proclaims adaptation via small concerted frequency shifts. To date the  
4 empirical evidence of clear sweep signals is more scarce than expected, while  
5 subtle shifts remain notoriously hard to detect. In the current study we develop  
6 a theoretical framework to predict the expected adaptive architecture of a trait,  
7 depending on parameters such as mutation rate, effective population size, size of  
8 the trait basis, and the available genetic variability at the onset of selection. For  
9 a population in mutation-selection-drift balance we find that adaptation proceeds  
10 via complete or partial sweeps for a large set of parameter values. We predict  
11 adaptation by small frequency shifts for two main cases. First, for traits with a  
12 large mutational target size and high levels of genetic redundancy among loci, and  
13 second if the starting frequencies of mutant alleles are more homogeneous than  
14 expected in mutation-selection-drift equilibrium, e.g. due to population structure  
15 or balancing selection.

# 16 2 Introduction

17 Rapid phenotypic adaptation of organisms to all kinds of novel environments is  
18 ubiquitous and has been described and studied for decades Barton and Keightley  
19 (2002); Messer et al. (2016). However, while the macroscopic changes of phenotypic  
20 traits are frequently evident, their genetic and genomic underpinnings are much  
21 more difficult to resolve. Two independent research traditions, molecular population  
22 genetics and quantitative genetics, have coined two opposite views of the adaptive  
23 process on the molecular level: adaptation either by selective sweeps or by subtle  
24 allele frequency shifts (*sweeps* or *shifts* from here on).

25 On the one hand, population genetics works bottom-up from the dynamics  
26 at single loci, without much focus on the phenotype. The implicit assumption  
27 of the sweep scenario is that selection on the trait results in sustained directional  
28 selection also on the level of single underlying loci. Consequently, we can observe  
29 phenotypic adaptation at the genotypic level, where selection drives allele frequencies  
30 at one or several loci from low values to high values. Large allele frequency  
31 changes are the hallmark of the sweep scenario. If these frequency changes  
32 occur in a short time interval, conspicuous diversity patterns in linked genomic  
33 regions emerge: the footprints of hard or soft selective sweeps Maynard-Smith  
34 and Haigh (1974); Kaplan et al. (1989); Barton (1998); Hermisson and Pennings  
35 (2017).

36 On the other hand, quantitative genetics envisions phenotypic adaptation top-down,  
37 from the vantage point of the trait. At the genetic level, it is perceived as a  
38 collective phenomenon that cannot easily be broken down to the contribution of  
39 single loci. Indeed, adaptation of a highly polygenic trait can result in a myriad of  
40 ways through “infinitesimally” small, correlated changes at the interacting loci of  
41 its basis (e.g. Boyle et al. (2017)). Conceptually, this view rests on the infinitesimal  
42 model by Fisher (1918) Fisher (1918) and its extensions (e.g. Barton et al.  
43 (2017)). Until a decade ago, the available moderate sample sizes for polymorphism  
44 data had strongly limited the statistical detectability of small frequency shifts.  
45 Therefore, the detection of sweeps with clear footprints was the major objective  
46 for many years. Since recently, however, huge sample sizes (primarily of human  
47 data) enable powerful genome-wide association studies (GWAS) to resolve the  
48 genomic basis of polygenic traits. Consequently, following conceptual work by  
49 Pritchard and coworkers Pritchard and Di Rienzo (2010); Pritchard et al. (2010),  
50 there has been a shift in focus to the detection of polygenic adaptation from  
51 subtle genomic signals (e.g. Hancock et al. (2010); Berg and Coop (2014);  
52 Field et al. (2016), reviewed in Csilléry et al. (2018)). Very recently, however,

53 some of the most prominent findings of polygenic adaptation in human height  
54 have been challenged Berg et al. (2018); Sohail et al. (2018). As it turned out,  
55 the methods are highly sensitive to confounding effects in GWAS data due to  
56 population stratification.

57 While discussion of the empirical evidence is ongoing, the key objective for  
58 theoretical population genetics is to clarify the conditions (mutation rates, selection  
59 pressures, genetic architecture) under which each adaptive scenario, sweeps,  
60 shifts – or any intermediate type – should be expected in the first place. Yet,  
61 the number of models in the literature that allow for a comparison of alternative  
62 adaptive scenarios at all is surprisingly limited (see also Stephan (2016)). Indeed,  
63 quantitative genetic studies based on the infinitesimal model or on summaries  
64 (moments, cumulants) of the breeding values do not resolve allele frequency  
65 changes at individual loci (e.g. Turelli and Barton (1990, 1994); Bürger and Lynch  
66 (1995); Bürger (2000)). In contrast, sweep models with a single locus under  
67 selection in the tradition of Maynard Smith and Haigh Maynard-Smith and Haigh  
68 (1974), or models based on adaptive walks or the adaptive dynamics framework  
69 (e.g. Geritz et al. (1998); Orr (2005); Matuszewski et al. (2015)) only allow for  
70 adaptive substitutions or sweeps. A notable exception is the pioneering study by  
71 Chevin and Hospital Chevin and Hospital (2008). Following Lande Lande (1983),  
72 these authors model adaptation at a single major quantitative trait locus (QTL)  
73 that interacts with an "infinitesimal background" of minor loci, which evolves with  
74 fixed genetic variance. Subsequent models Pavlidis et al. (2012); Wollstein and  
75 Stephan (2014) trace the allele frequency change at a single QTL in models with  
76 2-8 loci. Still, these articles do not discuss polygenic adaptation patterns. Most  
77 recently, Jain and Stephan Jain and Stephan (2015, 2017) studied the adaptive  
78 process for a quantitative trait under stabilizing selection with explicit genetic  
79 basis. Their analytical approach allows for a detailed view of allele frequency  
80 changes at all loci without constraining the genetic variance. However, the model

81 is deterministic and thus ignores the effects of genetic drift. Below, we study a  
82 polygenic trait that can adapt via sweeps or shifts under the action of all evolutionary  
83 forces (mutation, selection, recombination and drift). Our model allows for comprehensive  
84 analytical treatment, leading to a multi-locus, non-equilibrium extension of Wright's  
85 formula Wright (1931) for the joint distribution of allele frequencies at the end of  
86 the adaptive phase. This way, we obtain predictions concerning the adaptive  
87 architecture of polygenic traits and the population genetic variables that delimit  
88 the corresponding modes of adaptation.

89 The article is organized as follows. The Model section motivates our modeling  
90 decisions and describes the simulation method. We also give a brief intuitive  
91 account of our analytical approach. In the Results part, we describe our findings  
92 for a haploid trait with linkage equilibrium among loci. All our main conclusions  
93 in the Discussion part are based on the results displayed here. Further model  
94 extensions and complications (diploids, linkage, and alternative starting conditions)  
95 are relegated to appendices. Finally, we describe our analytical approach and  
96 derive all results in a comprehensive Mathematical Appendix. For the ease of  
97 reading, we have tried to keep both the main text and the Mathematical Appendix  
98 independent and largely self-contained.

### 99 **3 Model**

100 In the current study, we aim for a “minimal model” of a trait that allows us to clarify  
101 which evolutionary forces favor sweeps over shifts and vice versa (as well as any  
102 intermediate patterns). For shifts, alleles need to be able to hamper the rise of  
103 alleles at other loci via negative epistasis for fitness, e.g. diminishing returns  
104 epistasis. Indeed, otherwise one would only observe parallel sweeps. Negative  
105 fitness epistasis is frequently found in empirical studies (e.g. Kryazhimskiy et al.  
106 (2014)) and implicit to the Gaussian selection scheme used by (e.g. Chevin and

107 Hospital (2008); Jain and Stephan (2015, 2017)). More fundamentally, diminishing  
108 returns are a consequence of partial or complete redundancy of genetic effects  
109 across loci or gene pathways. Adaptive phenotypes (such as pathogen resistance  
110 or a beneficial body coloration) can often be produced in many alternative ways,  
111 such that redundancy is a common characteristic of beneficial mutations.

112 As our basic model, we focus on a haploid population and study adaptation  
113 for a polygenic, binary trait with full redundancy of effects at all loci. Any single  
114 mutation switches the phenotype from its ancestral state (e.g. “non-resistant”) to  
115 the adaptive state (“resistant”), further mutations have no additional effect. On  
116 the population level, adaptation can be produced by a single locus where the  
117 beneficial allele sweeps to fixation, or by small frequency shifts of alleles at many  
118 different loci in different individuals – or any combination. The symmetry among  
119 loci (no build-in advantage of any particular locus) and complete redundancy  
120 of locus effects provides us with a trait architecture that is most favorable for  
121 collective adaptation via small shifts – and with a modeling framework that allows  
122 for analytical treatment. The same model has been used in a preliminary simulation  
123 study Hermisson and Pennings (2017). In the context of parallel adaptation in a  
124 spatially structured population, analogous model assumptions with redundant loci  
125 have been used Ralph and Coop (2010, 2015); Paulose et al. (2018). In a second  
126 step, we extend our basic model to relax the redundancy condition, as described  
127 below.

### 128 **3.1 Basic model**

129 Consider a panmictic population of  $N_e$  haploids, with a binary trait  $Z$  (with phenotypic  
130 states  $Z_0$  “non-resistant” and  $Z_1$  “resistant”, see Fig 1). The trait is governed by  
131 a polygenic basis of  $L$  bi-allelic loci with arbitrary linkage (we treat the case of  
132 linkage equilibrium in the main text and analyze the effects of linkage in Appendix A.1).  
133 Only the genotype with the ancestral alleles at all loci produces phenotype  $Z_0$ , all

134 other genotypes produce  $Z_1$ , irrespective of the number of mutations they carry.  
135 Loci mutate at rate  $\mu_i$ ,  $1 \leq i \leq L$ , per generation (population mutation rate at  
136 the  $i$ th locus:  $2N_e\mu_i = \Theta_i$ ) from the ancestral to the derived allele. We ignore  
137 back mutation. The mutant phenotype  $Z_1$  is deleterious before time  $t = 0$ , when  
138 the population experiences a sudden change in the environment (e.g. arrival of  
139 a pathogen).  $Z_1$  is beneficial for time  $t > 0$ . The Malthusian (logarithmic) fitness  
140 function of an individual with phenotype  $Z$  reads

$$W(Z) = \begin{cases} s_d Z & \text{for } t < 0 \\ s_b Z & \text{for } t \geq 0. \end{cases} \quad (1)$$

141 Without restriction, we can assume  $Z_0 = 0$  and  $Z_1 = 1$ . Then  $W(Z_0) = 0$   
142 and  $W(Z_1) = s_d < 0$ , respectively  $W(Z_1) = s_b > 0$ , measure the strength of  
143 directional selection on  $Z$  (e.g. cost and benefit of resistance) before and after  
144 the environmental change. For the basic model, we assume that the population  
145 is in mutation-selection-drift equilibrium at time  $t = 0$ .

## 146 **3.2 Model extensions**

147 We extend the basic model in several directions. This includes linkage (Appendix A.1),  
148 alternative starting conditions at time  $t = 0$  (Appendix A.2), diploids (Appendix A.3),  
149 and arbitrary time-dependent selection  $s(t)$  (Mathematical Appendix M.1). Here,  
150 we describe how we relax the assumption of complete redundancy of all loci.  
151 Diminishing returns epistasis, e.g. due to Michaelis-Menten enzyme kinetics,  
152 will frequently not lead to complete adaptation in a single step, but may require  
153 multiple steps before the trait optimum is approached. In a model of incomplete  
154 redundancy, we thus assume that a first beneficial mutation only leads to partial  
155 adaptation. We thus have three states of the trait, the ancestral state for the  
156 genotype without mutations,  $Z_0 = 0$  (non-resistant), a phenotype  $Z_\delta = \delta$  (partially



157 resistant) for genotypes with a single mutation, and the mutant state  $Z_1 = 1$   
 158 (fully resistant) for all genotypes with at least two mutations, see Fig 1(b). For  
 159 diminishing returns epistasis, we require  $\frac{1}{2} \leq \delta < 1$ . The fitness function is as in  
 160 Eq (1).

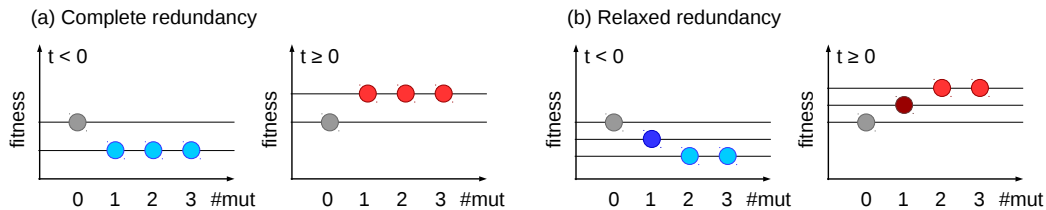


Figure 1: **Fitness schemes.** The fitness for individuals carrying 0, 1, 2, 3... mutations (y-axis) are given for the complete redundancy (a) and relaxed redundancy (b) model of fitness effects, respectively. Grey balls show the fitness of ancestral wild-type individuals (without mutations). Colored balls represent individuals carrying at least one mutation, for time points  $t < 0$  before the environmental change in blue and for  $t \geq 0$  in red.

### 161 3.3 Simulation model

162 For the models described above, we use Wright-Fisher simulations for a haploid,  
 163 panmictic populations of size  $N_e$ , assuming linkage equilibrium between all  $L$  loci  
 164 in discrete time. Selection and drift are implemented by independent weighted  
 165 sampling based on the marginal fitnesses of the ancestral and mutant alleles at  
 166 each locus. Due to linkage equilibrium, the marginal fitnesses only depend on  
 167 the allele frequencies. Ancestral alleles mutate with probability  $\mu_i$  per generation  
 168 at locus  $i$ . We start our simulations with a population that is monomorphic for  
 169 the ancestral allele at all loci. The population evolves for  $8N_e$  generations under  
 170 mutation and deleterious selection to reach (approximate) mutation-selection-drift  
 171 equilibrium. Following Hermisson and Pennings (2005, 2017), we condition on  
 172 adaptation from the ancestral state and discard all runs where the deleterious

173 mutant allele (at any locus) reaches fixation during this time. (We do not show  
174 results for cases with very high mutation rates and weak deleterious selection  
175 when most runs are discarded). At the time of environmental change, selection  
176 switches from negative to positive and simulation runs are continued until a prescribed  
177 stopping condition is reached.

178 We are interested in the genetic architecture of adaptation – the joint distribution  
179 of mutant frequencies across all loci – at the end of the rapid adaptive phase.  
180 Following Jain and Stephan (2017), we define this phase as “the time until the  
181 phenotypic mean reaches a value close to the new optimum”. Specifically, we  
182 stop simulations when the mean fitness  $\bar{W}$  in the population has increased up  
183 to a proportion  $f_w$  of the maximal attainable increase from the ancestral to the  
184 derived state,

$$\frac{W(Z_1) - \bar{W}}{W(Z_1) - W(Z_0)} = f_w. \quad (2)$$

185 For the basic model with complete redundancy, this simply corresponds to a  
186 residual proportion  $f_w$  of individuals with ancestral phenotype in the population.  
187 Extensions of the simulation scheme to include linkage or diploid individuals are  
188 described in Appendices A.1 and A.3.

189 *Parameter choices:* Unless explicitly stated otherwise, we simulate  $N_e =$   
190 10 000 individuals, with beneficial selection coefficients  $s_b = 0.1$  and  $0.01$ , combined  
191 with deleterious selection coefficients  $s_d = -0.1$  and  $s_d = -0.001$  for low and  
192 high levels of SGV, respectively. (The corresponding Wrightian fitness values  
193 used as sampling weights in discrete time are  $1 + s_b$  and  $1 + s_d$ .) We investigate  
194  $L = 2$  to 100 loci. We usually assume equal mutation rates at all loci,  $\mu_i = \mu$  and  
195 define  $\Theta_l = 2N_e\mu$  as the locus mutation parameter. Mutation rates are chosen  
196 such that the background mutation rates  $\Theta_{bg} := 2N_e\mu(L - 1)$  (detailed below in  
197 Eq (10)) takes values from 0.01 to 100. We typically simulate 10 000 replicates  
198 per mutation rate and stop simulations when the population has reached the new  
199 fitness optimum up to  $f_w = 0.05$ . In the model with complete redundancy, we thus

200 stop simulations when the frequency of individuals with mutant phenotype  $Z_1$  has  
201 increased to 95%.

### 202 **3.4 Analytical analysis**

203 We partition the adaptive process into two phases (see Fig 2 for illustration). An  
204 initial *stochastic phase*, governed by selection, drift, and mutation describes the  
205 establishment of mutant alleles at all loci. The subsequent *deterministic phase*  
206 governs the further evolution of established alleles until the end of the rapid  
207 adaptive phase as defined above. While mutation and drift can be ignored during  
208 the deterministic phase, interaction effects due to epistasis and linkage become  
209 important (in our model, they enter, in particular, through the stopping condition).  
210 We give a brief overview of our analytical approach below. A detailed account  
211 with the derivation of all results is provided in the Mathematical Appendix.

212 During the *stochastic phase*, we model the origin and spread of mutant copies  
213 as a so-called *Yule pure birth process* following Etheridge et al. (2006) and Hermisson  
214 and Pfaffelhuber (2008). The idea of this approach is that we only need to keep  
215 track of mutations that found “immortal lineages”, i.e. derived alleles that still  
216 have surviving offspring at the time of observation (see Fig 2 for the case of  
217  $L = 2$  loci). Forward in time, new immortal lineages can be created by two types  
218 of events: new mutations at all loci start new lineages, while birth events lead  
219 to splits of existing lineages into two immortal lineages. For  $t > 0$  (after the  
220 environmental change), in particular, new mutations at the  $i$ th locus arise at rate  
221  $N_e \mu_i$  per generation and are destined to become established in the population  
222 with probability  $\approx 2s_b$ . Simultaneously, existing beneficial mutant alleles at all  
223 loci spread at rate  $s_b$  (due to positive selection, via birth events exceeding death  
224 events). For the origin of new immortal lineages in the Yule process and their

225 subsequent splitting we thus obtain the rates

$$p_{\text{mut},i} \approx N_e \mu_i \cdot 2s_b = \Theta_i s_b \quad ; \quad p_{\text{split}} \approx s_b. \quad (3)$$

226 Extended results including standing genetic variation and time-dependent fitness  
 227 are given in the Appendix. Assume now that there are currently  $\{k_1, \dots, k_L\}$ ,  $0 \leq$   
 228  $k_j \ll N_e$  mutant lineages at the  $L$  loci. Then the probability that the next event in  
 229 the Yule process is either a birth (split) or a new mutation at locus  $i$  is

$$\frac{k_i \cdot p_{\text{split}} + p_{\text{mut},i}}{\sum_{j=1}^L (k_j \cdot p_{\text{split}} + p_{\text{mut},j})} = \frac{k_i + \Theta_i}{\sum_{j=1}^L (k_j + \Theta_j)}. \quad (4)$$

230 Importantly, all these transition probabilities among states of the Yule process  
 231 are constant in time and independent of the mutant fitness  $s_b$ , which cancels in  
 232 the ratio of the rates. As the number of lineages at all loci increases, their joint  
 233 distribution (across replicate realizations of the Yule process) approaches a limit.  
 234 In particular, as shown in the Appendix, the joint distribution of frequency ratios  
 235  $x_i := k_i/k_1$  in the limit  $k_1 \rightarrow \infty$  is given by an *inverted Dirichlet distribution*

$$P_{\text{inDir}}[\mathbf{x}|\Theta] = \frac{1}{B[\Theta]} \prod_{j=2}^L x_j^{\Theta_j-1} \left(1 + \sum_{i=2}^L x_i\right)^{-\sum_{i=1}^L \Theta_i} \quad (5)$$

236 where  $\mathbf{x} = (x_2, \dots, x_L)$  and  $\Theta = (\Theta_1, \dots, \Theta_L)$  are vectors of frequency ratios and  
 237 locus mutation rates, respectively, and where  $B[\Theta] = \frac{\prod_{j=1}^L \Gamma(\Theta_j)}{\sum_{j=1}^L \Gamma(\Theta_j)}$  is the generalized  
 238 Beta function and  $\Gamma(z)$  is the Gamma function. Note that Eq (5) depends only on  
 239 the locus mutation rates, but not on selection strength.

240 After the initial stochastic phase, when mutant lineages have established and  
 241 evaded stochastic loss, the dynamics can be adequately described by deterministic  
 242 selection equations. For allele frequencies  $p_i$  at locus  $i$ , assuming linkage equilibrium,

243 we obtain (consult the Mathematical Appendix M.1 for detailed derivations)

$$\dot{p}_i = p_i(W(Z_1) - \bar{W}) = s_b p_i(Z_1 - \bar{Z}), \quad (6)$$

244 where  $\bar{W}$  and  $\bar{Z}$  are population mean fitness and mean trait value. For the mutant  
245 frequency ratios  $x_i = p_i/p_1$ , we obtain

$$\dot{x}_i = \frac{d}{dt} \left( \frac{p_i}{p_1} \right) = \frac{\dot{p}_i p_1 - p_i \dot{p}_1}{p_1^2} = 0. \quad (7)$$

246 We thus conclude that the frequency ratios  $x_i$  do not change during the deterministic  
247 phase. In particular, this means that Eq (5) still holds at our time of observation at  
248 the end of the rapid adaptive phase. As shown in the Appendix, this is even true  
249 with linked loci. Finally, derivation of the joint distribution of mutant frequencies  $p_i$   
250 (instead of frequency ratios  $x_i$ ) at the time of observation requires a transformation  
251 of the density. In general, this transformation depends on the stopping condition  
252  $f_w$  and on other factors such as linkage. Assuming linkage equilibrium among all  
253 selected loci, we obtain (see the Mathematical Appendix, Theorem 2, Eq (M.20))

$$\mathbf{P}_{f_w}[\mathbf{p}|\Theta] = \frac{\delta_{\prod_{j=1}^L (1-p_j) - f_w}}{B[\Theta]} \prod_{j=1}^L p_j^{\Theta_j - 1} \left( \sum_{i=1}^L p_i \right)^{-\sum_{i=1}^L \Theta_i} \left( \sum_{j=1}^L \frac{f_w p_j}{1 - p_j} \right) \quad (8)$$

254 for  $\mathbf{p} = (p_1, \dots, p_L)$  in the  $L$ -dimensional hypercube of allele frequencies. The  
255 delta function  $\delta_X$  restricts the distribution to the  $L-1$  dimensional manifold defined  
256 via the stopping condition  $f_w = \prod_{j=1}^L (1 - p_j)$ . Further expressions, also including  
257 linkage, are given in the Mathematical Appendix and in Appendix A.1. In general,  
258 the joint distribution corresponds to a family of generalized Dirichlet distributions  
259 depending on the stopping condition. In the special case  $f_w \rightarrow 0$  (i.e. complete  
260 adaptation, enforcing fixation at at least one locus), the distribution Eq (8) is  
261 restricted to a boundary face of the allele frequency hypercube and reduces to the  
262 inverted Dirichlet distribution given above in Eq (5). In the results section below,

263 we assess our analytical approximations for the joint distributions of adaptive  
 264 alleles, Eq (5) and Eq (8), and discuss their implications in the context of scenarios  
 265 of polygenic adaptation, ranging from sweeps to small frequency shifts.

|  |     |   |
|--|-----|---|
| $L$  | ... | size of polygenic basis (no. of loci)                         |
| $s_d, s_b$   | ... | selection coefficient before/after the environment changes    |
| $p_i := \frac{k_i}{N}$   | ... | mutant allele frequency at locus $i$                          |
| $x_i := \frac{k_i}{k_1} = \frac{p_i}{p_1}$                                     | ... | mutant allele frequency ratio: locus $i$ / locus 1            |
| $f_w$  | ... | frequency of ancestral phenotype                              |
| $\mu_i$  | ... | allelic mutation rate at locus $i$                            |
| $\Theta_i = 2N_e\mu_i$   | ... | haploid population mutation rate at locus $i$                 |
| $\Theta = \{\Theta_1, \dots, \Theta_L\}$                                       | ... | vector of all locus population mutation rates                 |
| $\Theta_l$   | ... | locus pop. mut. rate, for model with equal mutation rates     |
| $\Theta_{bg}$  | ... | background mutation rate, Eq (10)                             |
| $B[\Theta] = \frac{\prod_{i>1} \Gamma(\Theta_i)}{\sum_{i>1} \Gamma(\Theta_i)}$ | ... | Beta function, where $\Gamma(\Theta_i)$ is the Gamma function |

Table 1: Glossary

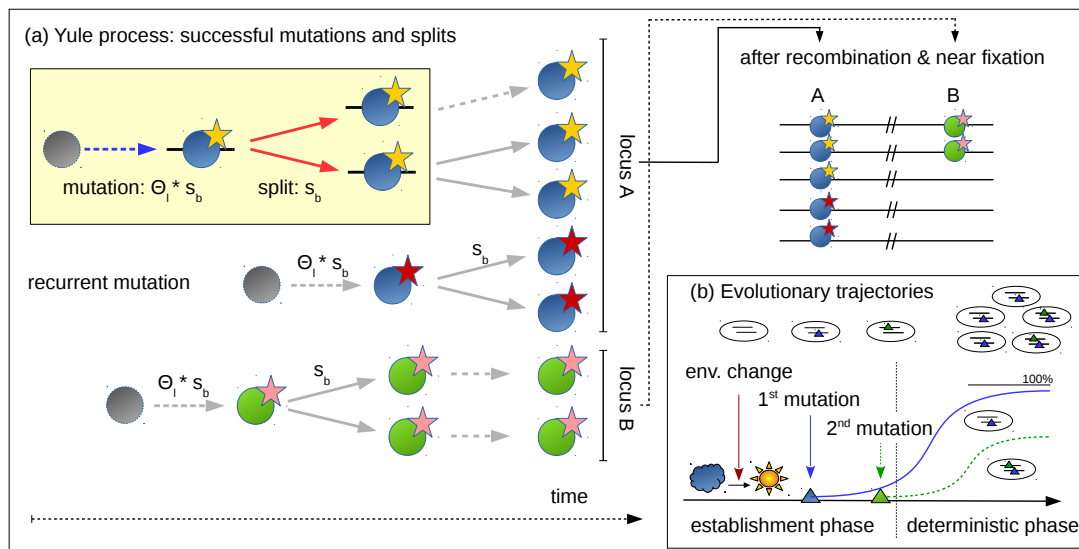


**Figure 2: Phases of polygenic adaptation.** The adaptive process is partitioned into two phases. The initial, stochastic phase describes the establishment of mutant alleles. Ignoring epistasis during this phase, it can be described by a *Yule* process (panel a), with two types of events (yellow box). Either a new mutation occurs and establishes with rate  $\Theta_l \cdot s_b$  or an existing mutant line splits into two daughter lines at rate  $s_b$ . Mutations and splits can occur in parallel at all loci of the polygenic basis, (here 2 loci, shown in green and blue). Yellow and red stars at the blue locus indicate establishment of two recurrent mutations at this locus. When mutants have grown to larger frequencies, the adaptive process enters its second, deterministic phase, where drift can be ignored (panel b). During the deterministic phase, the trajectories of mutations at different loci constrain each other due to epistasis. We refer to the locus ending up at the highest frequency as the *major* locus (here in blue) and to all others as *minor* loci (here one in green).

## 266 4 Results

267 While the joint distribution of allele frequencies provides comprehensive information  
268 of the adaptive architecture, low-dimensional summary statistics of this distribution  
269 are needed to describe and classify distinct types of polygenic adaptation. To  
270 this end, we order loci according to their contribution to the adaptive response.  
271 In particular, we call the locus with the largest allele frequency at the stopping  
272 condition the *major locus* and all other loci *minor loci*. Minor loci are further  
273 ordered according to their frequency (first minor, second minor, etc.). The marginal  
274 distributions of the major locus or  $k$ th minor locus are 1-dim summaries of the joint  
275 distribution. Importantly, these summaries are still *collective* because the role of  
276 any specific locus (its order) is defined through the allele frequency changes at  
277 *all* loci. This is different for the marginal distribution at a fixed focal locus, which  
278 is chosen irrespective of its role in the adaptive process, e.g. Chevin and Hospital  
279 (2008); Pavlidis et al. (2012); Wollstein and Stephan (2014).

280 Concerning our nomenclature, note, that the *major* and *minor* loci do not differ  
281 in their effect size, as they are completely redundant. Still, the major locus is the  
282 one with the largest contribution to the adaptive response and would yield the  
283 strongest association in a GWAS case-control study.

284 In the following, we analyze adaptive trait architectures in three steps. In  
285 Section 4.1 we use the expected allele frequency ratio of minor and major loci as a  
286 one-dimensional summary statistic. Subsequently, in Section 4.2, we analyze the  
287 marginal distributions of major and minor loci for a fully redundant trait with 2 to  
288 100 loci. Finally, in Section 4.3 we investigate the robustness of our results under  
289 conditions of relaxed redundancy. Further results devoted to diploids, linkage,  
290 and alternative starting conditions are provided in the Appendices.



## 291 4.1 Expected allele frequency ratio

292 For our biological question concerning the type of polygenic adaptation, the ratio  
293 of allele frequency changes of minor over major loci is particularly useful. With  
294 “sweeps at few loci”, we expect large differences among loci, resulting in ratios  
295 that deviate strongly from 1. In contrast, with “subtle shifts at many loci”, allele  
296 frequency shifts across loci should be similar, and ratios should range close to  
297 1. Our theory (explained above) predicts that these ratios are the outcome of  
298 the stochastic phase, yet their distribution is preserved during the deterministic  
299 phase. They are thus independent of the precise time of observation. For our  
300 results in this section, we assume that the mutation rate at all  $L$  loci is equal,  
301  $\Theta_i \equiv \Theta_l$ , for all  $1 \leq i \leq L$ . This corresponds to the symmetric case that is most  
302 favorable for a “small shift” scenario.

303 Consider first the case of  $L = 2$  loci. There is then a single allele frequency  
304 ratio “minor over major locus”, which we denote by  $x$ . For two loci, the joint  
305 distribution of frequency ratios from Eq (5) reduces to a *beta-prime* distribution.  
306 Conditioning on the case that the first locus is the major locus (probability  $1/2$  for  
307 the symmetric model), we obtain for  $0 \leq x \leq 1$ ,

$$P_{\beta'}[x|\Theta_l] = \frac{2\Gamma(2\Theta_l)}{(\Gamma(\Theta_l))^2} x^{\Theta_l-1}(1+x)^{-2\Theta_l}, \quad (9)$$

308 Fig 3 compares the expectation of this analytical prediction with simulation  
309 results for a range of parameters for the strength of beneficial selection  $s_b$  and for  
310 the level of standing genetic variation (implicitly given by the strength of deleterious  
311 selection  $s_d$  before the environmental change). There are two main observations.  
312 First, the simulation results demonstrate the importance of the scaled mutation  
313 rate  $\Theta_{bg} \equiv \Theta_l$  (for two loci). Low  $\Theta_{bg}$  leads to sweep-like adaptation (heterogeneous  
314 adaptation response among loci,  $E[x] \ll 1$ ), whereas high  $\Theta_{bg}$  leads to shift-like  
315 adaptation (homogeneous response,  $E[x]$  near 1). Second, the panels show that

316 the selection intensity given by  $s_d$  and  $s_b$  has virtually no effect. Both results are  
317 predicted by the analytical theory (Eq (9)). In Appendix A.1, we further show that  
318 these results hold for arbitrary degrees of linkage (including complete linkage),  
319 see Fig S.1.

320 For more than two loci,  $L > 2$ , one-dimensional marginal distributions of the  
321 joint distribution, Eq (5), generally require  $(L - 1)$ -fold integration, which can  
322 be complicated. However, it turns out that the key phenomena to characterize  
323 the adaptive architecture can still be captured by the 2-locus formalism, with  
324 appropriate rescaling of the mutation rate. For the general  $L$ -locus model, we  
325 broaden our definition of the summary statistic  $x$  above to describe the allele  
326 frequency ratio of the *first minor* locus and the major locus. To relate the distribution  
327 of  $x$  in the  $L$ -locus model to the one in the 2-locus model, we reason as follows:  
328 For small locus mutation rates  $\Theta_l$ , the order of the loci is largely determined  
329 by the order at which mutations establish at these loci. *I.e.*, the locus where  
330 the first mutation establishes ends up as the major locus and the first minor  
331 locus is usually the second locus where a mutation establishes. The distribution  
332 of the allele frequency ratio  $x$  is primarily determined by the distribution of the  
333 waiting time for this second mutation after establishment of the first mutation at  
334 the major locus. In the 2-locus model, this time will be exponentially distributed,  
335 with parameter  $1/\Theta_l$ . In the  $L$ -locus model, however, where  $L - 1$  loci with total  
336 mutation rate  $\Theta_l(L - 1)$  compete for being the “first minor”, the parameter for the  
337 waiting-time distribution reduces to  $1/(\Theta_l(L - 1))$ . We thus see from this argument  
338 that the decisive parameter is the cumulative *background mutation rate*

$$\Theta_{bg} = (L - 1)\Theta_l \quad (10)$$

339 at all minor loci in the background of the major locus. In Fig 3 (orange dots) we  
340 show simulations of a  $L = 10$  locus model with an appropriately rescaled locus

341 mutation rate  $\Theta_l \rightarrow \Theta_l/9$ , such that the background rate  $\Theta_{bg}$  is the same as for the  
 342 2-locus model. We see that the analytical prediction based on the 2-locus model  
 343 provides a good fit for the 10-locus model. A more detailed discussion of this type  
 344 of approximation is given in Appendix A.4.

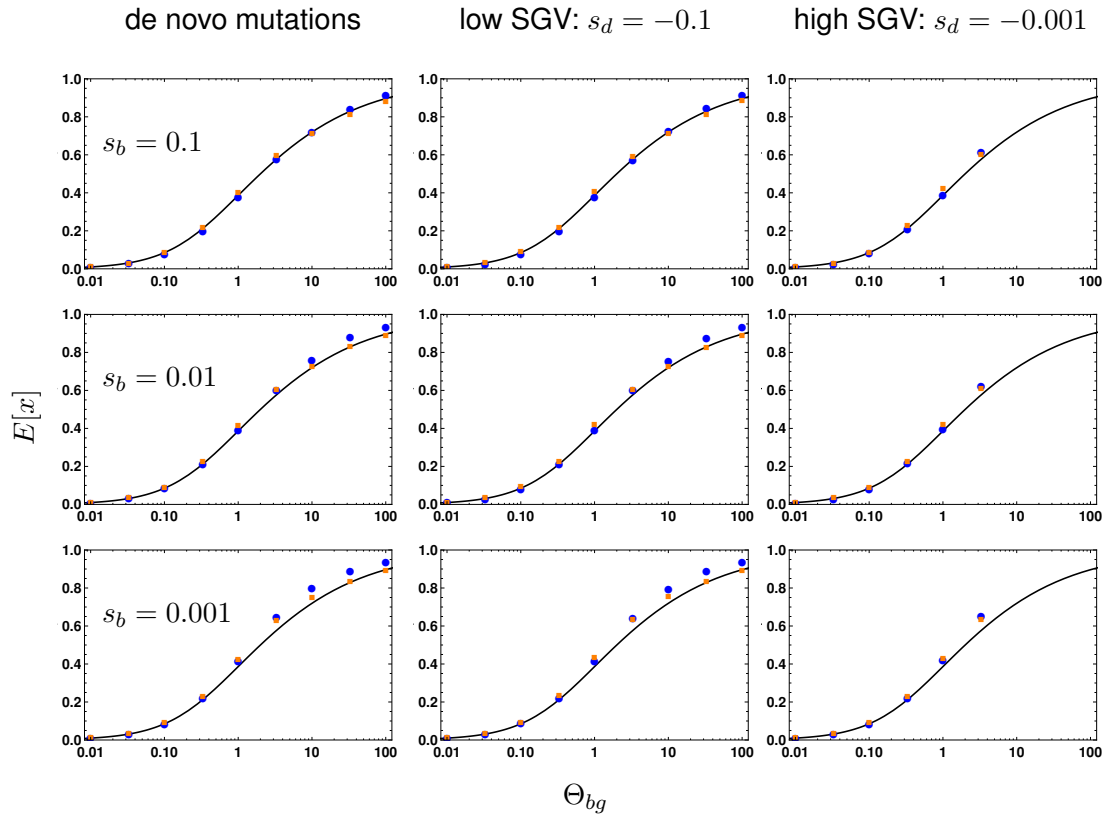


**Figure 3: Effect of selection strength and SGV on the frequency ratio  $E[x]$ .** We contrast the expected allele frequency ratios of the first minor locus (with the second largest frequency) over the major locus (with the largest frequency) for 2 loci (blue dots) and for 10 loci (orange dots) with analytical predictions (Appendix, Eq M.16, black curve).  $E[x]$  is shown as a function of  $\Theta_{bg}$  ( $= \Theta_l$  for the 2-locus case). Panels correspond to different strengths of positive selection ( $s_b$ , rows) and levels of SGV (no SGV, strongly deleterious  $s_d = 0.1$ , weakly deleterious  $s_d = 0.001$ , columns). We find that neither factor alters the expected ratio. We do not obtain results for all parameters, as we condition on adaptation from ancestral alleles, such that simulation runs are discarded if sampling conditions are met before the environmental change. Results for 10 000 replicates, standard errors  $< 0.005$  (smaller than symbols).

## 345 4.2 Genomic architecture of polygenic adaptation

346 While the distribution of allele frequency ratios, Eqs (5) and (9), offers a coarse  
347 (but robust) descriptor of the adaptive scenario, the joint distribution of allele  
348 frequencies at the end of the adaptive phase, Eq (8), allows for a more refined  
349 view. In contrast to the distribution of ratios, the results now depend explicitly on  
350 the stopping condition (the time of observation) and on linkage among loci. We  
351 assume linkage equilibrium in this section and assess the mutant allele frequencies  
352 when the frequency of the remaining wild-type individuals in the population is  $f_w$   
353 (= 0.05 in our figures).

354 Fig 4 displays the main result of this section. It shows the marginal distributions  
355 of all loci, ordered according to their allele frequency at the time of observation  
356 (major locus, 1st, 2nd, 3rd minor locus, *etc.*) for traits with  $L = 2, 10, 50,$  and  
357 100 loci. Panels in the same row correspond to equal background mutation  
358 rates  $\Theta_{bg} = (L - 1)\Theta_l$ , but note that the locus mutation rates  $\Theta_l$  are not equal.  
359 The figure reveals a striking level of uniformity of adaptive architectures with the  
360 same  $\Theta_{bg}$ , but vastly different number of loci. For  $\Theta_{bg} \leq 1$  (the first three rows),  
361 the marginal distributions for loci of the same order (same color in the Figure)  
362 across traits with different  $L$  is almost invariant. For large  $\Theta_{bg}$ , they converge  
363 for sufficiently large  $L$  (e.g. for  $\Theta_{bg} = 10$ , going from  $L = 10$  to  $L = 50$  and to  
364  $L = 100$ ). In particular, the background mutation rate  $\Theta_{bg}$  determines the shape  
365 of the major-locus distribution (red in the Figure) for large  $p \rightarrow 1 - f_w = 0.95$  (the  
366 maximum possible frequency, given the stopping condition). For  $\Theta_{bg} < 1$ , this  
367 distribution is sharply peaked with a singularity at  $p = 1 - f_w$ , whereas it drops to  
368 zero for large  $p$  if  $\Theta_{bg} > 1$  (see also the analytical results below).

369 As predicted by the theory, Eq (8) and below, simulations (not shown) confirm  
370 that selection parameters do not affect the adaptive architecture. As discussed in  
371 Appendix A.1, sufficiently tight linkage does change the shape of the distributions.

372 Importantly, however, it does not affect the role of  $\Theta_{bg}$  in determining the singularity  
373 of the major-locus distribution. This confirms the key role of the background  
374 mutation rate as a single parameter to determine the adaptive scenario in our  
375 model. While  $\Theta_{bg} = 1$  separates architectures that are dominated by a single  
376 major locus ( $\Theta_{bg} < 1$ ) from collective scenarios (with  $\Theta_{bg} > 1$ ), the classical sweep  
377 or shift scenarios are only obtained if  $\Theta_{bg}$  deviates strongly from 1. We therefore  
378 distinguish three adaptive scenarios.

- 379 •  $\Theta_{bg} \lesssim 0.1$ , *single completed sweeps*. For  $\Theta_{bg} \ll 1$  (first two rows of Fig 4),  
380 the distribution of the major locus is concentrated at the maximum of its  
381 range, while all other distributions are concentrated around 0. Adaptation  
382 thus occurs at a single locus, via a selective sweep from low to high mutant  
383 frequency. Contributions by further loci are rare. If they occur at all they are  
384 usually due to a single runner-up locus (the largest minor locus).
- 385 •  $0.1 < \Theta_{bg} < 100$ , *heterogeneous partial sweeps*. With intermediate background  
386 mutation rates (third and fourth row of Fig 4), we still observe a strong asymmetry  
387 in the frequency spectrum. Even for values of  $\Theta_{bg}$  slightly larger than 1, there  
388 is a clear major locus discernible, with most of its distribution for  $p > 0.5$ .  
389 However, there is also a significant contribution of several minor loci that  
390 rise to intermediate frequencies. We thus obtain a heterogeneous pattern  
391 of partial sweeps at a limited number of loci.
- 392 •  $\Theta_{bg} \gtrsim 100$ , *homogeneous frequency shifts*. Only for high background  
393 mutation rates  $\Theta_{bg} \gg 1$  (last row of Fig 4 with  $\Theta_{bg} = 100$ ), the heterogeneity  
394 in the locus contributions to the adaptive response vanishes. There is then  
395 no dominating major locus. For only 2 loci, these shifts are necessarily still  
396 quite large, but for traits with a large genetic basis (large  $L$ ; the only realistic  
397 case for high values of  $\Theta_{bg}$ ), adaptation occurs via subtle frequency shifts at  
398 many loci.

### 399 Analytical predictions

400 To gain deeper understanding of the polygenic architecture – and for quantitative  
 401 predictions – we dissect our analytical result for the joint frequency spectrum in  
 402 Eq (8). We start with the case of  $L = 2$  loci, allowing for different locus mutation  
 403 rates  $\Theta_1$  and  $\Theta_2$ . The marginal distribution at the first locus reads (from Eq (8),  
 404 after integration over  $p_2$ ),

$$P_{f_w}[p_1|\Theta_1, \Theta_2] = \frac{p_1^{\Theta_1-1}(1-p_1-f_w)^{\Theta_2-1}(1-p_1)^{\Theta_1+1}}{B[\Theta_1, \Theta_2](1-p_1^2-f_w)^{\Theta_1+\Theta_2}} \left(1 - \frac{f_w(1-2p_1)}{(1-p_1)^2}\right), \quad (11)$$

405 for  $0 \leq p_1 \leq 1 - f_w$  (see also Appendix A.5). The distribution has a singularity at  
 406  $p_1 = 0$  if the corresponding *locus* mutation rate is smaller than one,  $\Theta_1 < 1$ . It has  
 407 a singularity at  $p_1 = 1 - f_w$  if the corresponding *background* mutation rate (which  
 408 is just the mutation rate at the other locus for  $L = 2$ ) is smaller than one,  $\Theta_2 < 1$ .  
 409 The marginal distributions at the major locus,  $P_{f_w}^+[p|\Theta_1, \Theta_2]$ , and the minor locus,  
 410  $P_{f_w}^-[p|\Theta_1, \Theta_2]$ , follow from Eq (11) as

$$P_{f_w}^\pm[p|\Theta_1, \Theta_2] = P_{f_w}[p|\Theta_1, \Theta_2] + P_{f_w}[p|\Theta_2, \Theta_1], \quad (12)$$

411 where  $P_{f_w}^+[p|\Theta_1, \Theta_2]$  is defined for  $1 - \sqrt{f_w} \leq p \leq 1 - f_w$  and  $P_{f_w}^-[p|\Theta_1, \Theta_2]$  is  
 412 defined for  $0 \leq p \leq 1 - \sqrt{f_w}$ . The sum in Eq (12) accounts for the alternative  
 413 events that either the first locus or the second may end up as the major (or minor)  
 414 locus. Consequently,  $P_{f_w}^-[p|\Theta_1, \Theta_2]$  has a singularity at  $p = 0$  if the *minimal locus*  
 415 *mutation rate*  $\Theta_l = \min[\Theta_1, \Theta_2] < 1$ . Analogously,  $P_{f_w}^+[p|\Theta_1, \Theta_2]$  has a singularity  
 416 at  $p = 1 - f_w$  if the *minimal background mutation rate*  $\Theta_{bg} = \min[\Theta_1, \Theta_2] < 1$ . The  
 417 left column of Fig 4 shows the distributions at the major and minor locus for  $L = 2$   
 418 in the symmetric case  $\Theta_1 = \Theta_2 = \Theta_l = \Theta_{bg}$  and  $f_w = 0.05$ . Simulations for a  
 419 population of size  $N_e = 10\,000$  and analytical predictions match well.

420 How do these results generalize for  $L > 2$ ? We again allow for unequal locus

421 mutation rates  $\Theta_i$ . It is easy to see from Eq (8) that the marginal distribution at the  
 422  $i$ th locus has a singularity at  $p_i = 0$  for  $\Theta_i < 1$ . In the Mathematical Appendix M.3,  
 423 we further show that it has a second singularity at  $p_i = 1 - f_w$  if the corresponding  
 424 background mutation rate  $\sum_{j \neq i}^d \Theta_j$  is smaller than 1. As a first step, we split the  
 425 joint distribution, Eq (8), into the marginal distribution at the major locus  $P_{f_w}^+[p|\Theta]$   
 426 (defined for  $1 - \sqrt[L]{f_w} \leq p \leq 1 - f_w$ ) and a cumulative distribution at all other (minor)  
 427 loci,  $P_{f_w}^- [p|\Theta]$  (defined for  $0 \leq p \leq 1 - \sqrt[L]{f_w}$ ). Since any locus can end up as the  
 428 major locus (with probability  $> 0$ ),  $P_{f_w}^+[p|\Theta]$  has a singularity at  $p = 1 - f_w$  for

$$\Theta_{bg} := \min_{1 \leq i \leq L} \left[ \sum_{j=1}^L \Theta_j - \Theta_i \right] < 1. \quad (13)$$

429 This equation generalizes the definition of the background mutation rate, Eq (10),  
 430 to the case of unequal locus mutation rates. Similarly,  $P_{f_w}^- [p|\Theta]$  has a singularity  
 431 at  $p = 0$  if

$$\Theta_l := \min_{1 \leq i \leq L} [\Theta_i] < 1. \quad (14)$$

432 As long as  $\Theta_{bg} \leq 1$ , we can approximate both the major-locus distribution  $P_{f_w}^+[p|\Theta]$   
 433 and the cumulative minor locus distribution  $P_{f_w}^- [p|\Theta]$  for arbitrary  $L$  by formulas for  
 434 a 2-locus model with locus mutation rates matching  $\Theta_l$  and  $\Theta_{bg}$  of the multi-locus  
 435 model, Eq (12). Similarly, we can use results from a  $k$ -locus model to match the  
 436 marginal distributions of the largest  $k$  loci (i.e., up to the  $(k-1)$ th minor) in models  
 437 with  $L > k$  loci, upon rescaling of the mutation rates. As explained for the ratio  
 438 of the first minor and major locus in the previous section, rescaling rules match  
 439 the expected waiting time for establishment of a mutation at the  $k$ th locus after  
 440 establishment of a first mutation. Details are given in the Appendix A.4. In Fig 4,  
 441 we use formulas derived from a  $k$ -locus model ( $k \leq 4$ ) to approximate the  $(k-1)$ st  
 442 minor locus distribution of models with  $L = 10; 50; 100$  loci and  $\Theta_{bg} \leq 1$ . These  
 443 approximations work well as long as these leading loci dominate the adaptive  
 444 architecture of the trait, which is the case for  $\Theta_{bg} \leq 1$ .

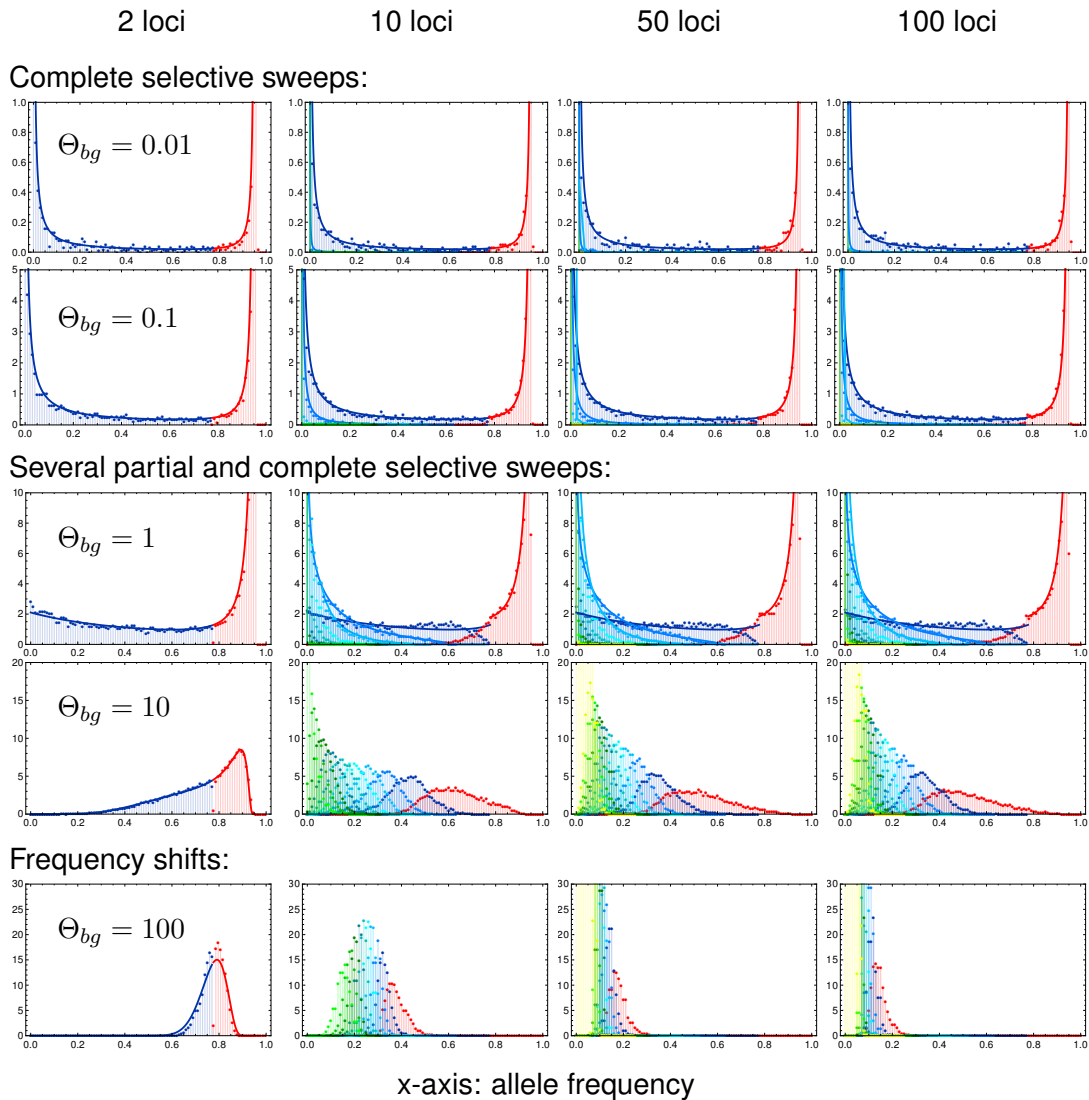


**Figure 4: Genomic architecture of polygenic adaptation.** We distinguish three patterns of architectures with increasing genomic background mutation rate  $\Theta_{bg}$ : complete sweeps, for  $\Theta_{bg} \lesssim 0.1$ , heterogeneous partial sweeps at several loci for  $0.1 < \Theta_{bg} < 100$ , and polygenic frequency shifts for  $\Theta_{bg} \gtrsim 100$ . The plots show the marginal distributions of all loci, ordered according to their allele frequency, i.e. the major locus in red and all following (first, second, third, etc. minors) in blue to green. Lines in respective colors show analytical predictions, Appendix A.4. Simulations were stopped once the populations have adapted to 95% of the maximum mean fitness in each of 10 000 replicates, resulting in an the upper bound for the major locus distribution at,  $p_1 = 0.95$ . Simulations for  $s_b = -s_d = 0.1$ . Note the different scaling of the y-axis for different mutation rates.

### 445 **4.3 Relaxing complete redundancy**

446 To complete our picture of adaptive architectures, we investigate the robustness  
 447 of our model assumption against relaxation of redundancy. As explained above



448 (*Model extensions* and Fig 1), we implement diminishing returns epistasis, such  
449 that an individual with a single mutation has fitness  $\delta s_{b/d}$ , while individuals carrying  
450 more than one mutation have fitness  $s_{b/d}$ . With small deviations from complete  
451 redundancy (e.g.  $\delta = 0.9$ , stopping at 5% ancestral phenotypes, data not shown)  
452 we obtain basically no differences in the genomic patterns of adaptation. With  
453 larger deviations (e.g.  $\delta = 0.5$ ) quantitative differences appear. However, the  
454 qualitative picture concerning the scenario of polygenic adaptation remains the  
455 same.

456 Fig 5 shows the marginal frequency distributions of major and minor loci for  
457 a trait with relaxed redundancy with  $\delta = 0.5$  that is sampled when the population  
458 has accomplished 95% of the fitness increase on its way to the new optimum,  
459 Eq (2). Given the fitness function, this is not possible with adaptation at only a  
460 single locus. At least two loci are needed. The Figure compares the simulation  
461 data for the relaxed redundancy model (colored dots) and the full redundancy  
462 model (dots in back and gray). As in Fig 4, traits in the same row have the same  
463 background mutation rate  $\Theta_{bg}$ . However, the background rate for the model with  
464 relaxed redundancy is redefined as

$$\Theta_{bg}^{\text{relax}} = (L - 2)\Theta_l \quad (15)$$

465 where  $\Theta_l$  is the locus mutation rate (equal at all loci). We thus define the background  
466 rate, more precisely, as the combined population-scaled mutation rate of all loci  
467 *that are not essential* to accomplish adaptation of the phenotype and, thus, are  
468 truly redundant. With this choice, the adaptive architecture of the relaxed redundancy  
469 model reproduces the one of the model with full redundancy – up to a shift in  
470 the number of the loci due to an extra locus that is needed for adaptation with  
471 relaxed redundancy. The Figure captures this by comparing traits with relaxed  
472 redundancy with  $L = 3, 4, 11$ , and 101 loci to fully redundant traits with one fewer

473 locus. The inset figures in the column for  $L = 4$  loci show the same scenario,  
474 but with an *averaged* marginal distribution for the two largest loci with relaxed  
475 redundancy (in green).

476 • For mutation rates,  $\Theta_{bg} \ll 1$ , we still find adaptation by sweeps. Relative to  
477 the full redundancy model, we now observe two “major” sweep loci instead  
478 of only a single sweep. The inset (for  $L = 4$ ) shows that their averaged  
479 distributions matches the major locus distribution of the full redundancy  
480 model. The distribution at the third largest locus (the “first minor” locus  
481 with relaxed redundancy) resembles the corresponding distribution of the  
482 first minor locus of the trait with full redundancy.

483 • For intermediate mutation rates,  $0.1 < \Theta_{bg} < 100$ , the pattern is dominated  
484 by partial sweeps. We clearly see the similarity in the marginal distributions  
485 of the  $k$ th largest locus with full redundancy and the  $k + 1$ st largest locus of  
486 the relaxed redundancy trait. For the two major loci with relaxed redundancy,  
487 we again see (inset) that the averaged distribution matches the major-locus  
488 distribution of the full redundancy model.

489 • Finally, for strong mutation,  $\Theta_{bg} \gtrsim 100$ , adaptation again occurs by small  
490 frequency shifts at many loci.

491 In summary, our results show that relaxing redundancy leads to qualitatively  
492 similar results, but with a reduced “effective” background mutation rate that only  
493 accounts for “truly redundant” loci.

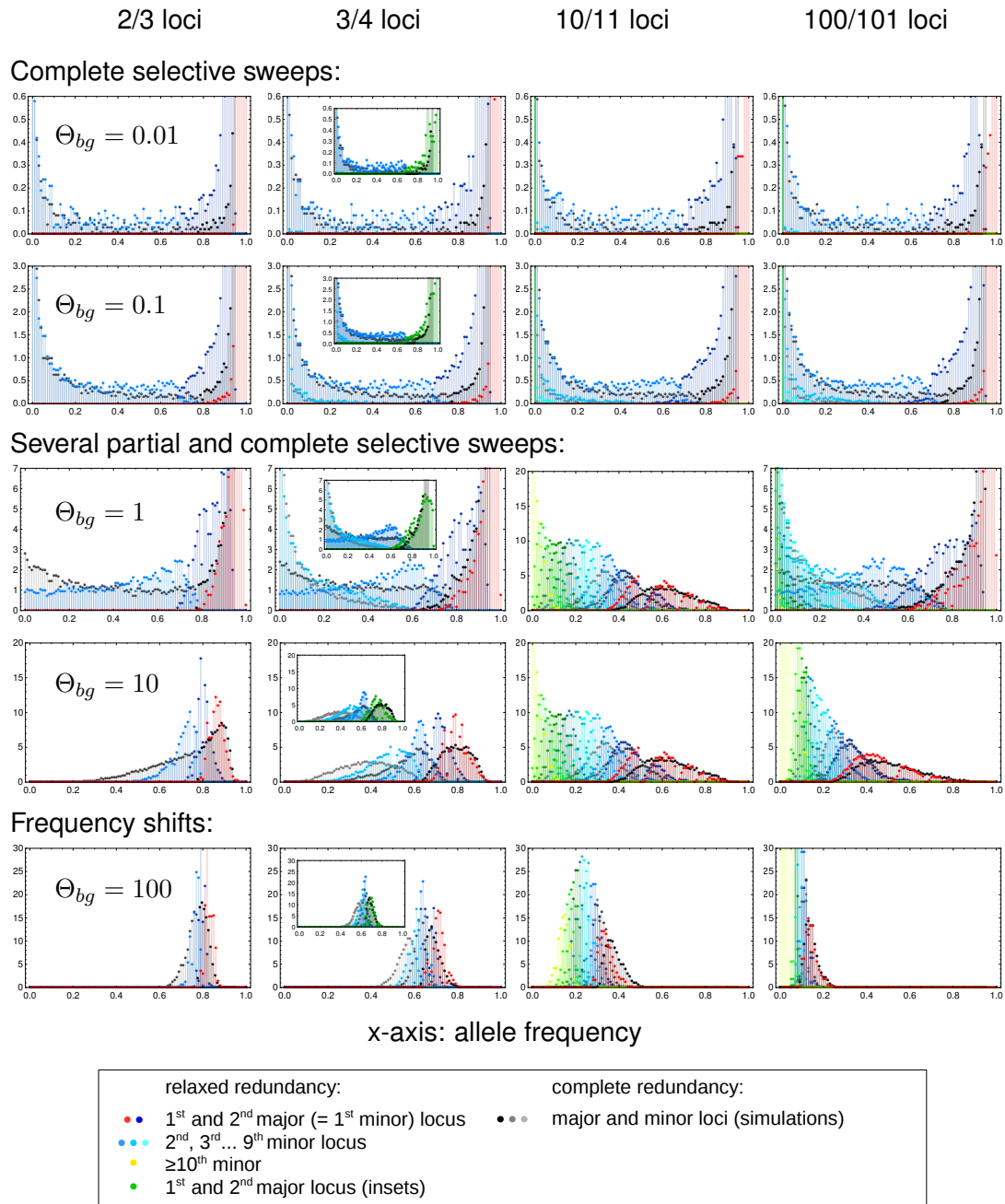


Figure 5: **Relaxed redundancy.** Relaxing redundancy such that a single mutant has fitness  $1 + 0.5s_{b/d}$  and only two mutations or more confer the full fitness effect ( $1 + s_{b/d}$ ) demonstrates the robustness of our model. As in Fig 4, allele frequency distributions of derived alleles are displayed once the population has reached 95% of maximum attainable mean population fitness. Genomic patterns of adaptation show similar characteristics as with complete redundancy. Due to relaxed redundancy, an additional "major locus" is required to reach the adaptive optimum. As explained in the main text, the distribution of the  $k$ th largest locus with complete redundancy therefore corresponds to the distribution of the  $k + 1$ st largest locus with relaxed redundancy. Insets in the second column show the same data with the distributions of the two major loci for relaxed redundancy combined (in green).

## 494 **5 Discussion**

495 Traits with a polygenic basis can adapt in different ways. Few or many loci can  
496 contribute to the adaptive response. The changes in the allele frequencies at  
497 these loci can be large or small. They can be homogeneous or heterogeneous.  
498 While molecular population genetics posits large frequency changes – selective  
499 sweeps – at few loci, quantitative genetics views polygenic adaptation as a collective  
500 response, with small, homogeneous allele frequency shifts at many loci. Here,  
501 we have explored the conditions under which each adaptive scenario should be  
502 expected, analyzing a polygenic trait with redundancy among loci that allows for  
503 a full range of adaptive architectures: from sweeps to subtle frequency shifts.

### 504 **5.1 Polygenic architectures of adaptation**

505 For any polygenic trait, the multitude of possible adaptive architectures is fully  
506 captured by the joint distribution of mutant alleles across the loci in its basis.  
507 Different adaptive scenarios (such as sweeps or shifts) correspond to characteristic  
508 differences in the shape of this distribution, at the end of the adaptive phase. For  
509 a single locus, the stationary distribution under mutation, selection and drift can  
510 be derived from diffusion theory and has been known since the early days of  
511 population genetics (S. Wright (1931), Wright (1931)). For multiple interacting  
512 loci, however, this is usually not possible. To address this problem for our model,  
513 we dissect the adaptive process into two phases. The early stochastic phase  
514 describes the establishment of all mutants that contribute to the adaptive response  
515 under the influence of mutation and drift. We use that loci can be treated as  
516 independent during this phase to derive a joint distribution for ratios of allele  
517 frequencies at different loci, Eq (5). During the second, deterministic phase,  
518 epistasis and linkage become noticeable, but mutation and drift can be ignored.  
519 Allele frequency changes during this phase can be described as a density transformation

520 of the joint distribution. For the simple model with fully redundant loci, and assuming  
521 either LE or complete linkage, this transformation can be worked out explicitly.  
522 Our main result Eq (8) can thus be understood as a multi-locus extension of  
523 Wright’s stationary distribution. For a neutral locus with multiple alleles, Wright’s  
524 distribution is a Dirichlet distribution, which is reproduced in our model for the  
525 case of complete linkage, see Appendix A.1. For the opposite case of linkage  
526 equilibrium, we obtain a family of inverted Dirichlet distributions, depending on  
527 the stopping condition – our time of observation.

528 Note that the distribution of adaptive architectures is *not* a stationary distribution,  
529 but necessarily transient. It describes the pattern of mutant alleles at the end of  
530 the “rapid adaptive phase” Jain and Stephan (2015, 2017), because this is the  
531 time scale that the opposite narratives of population genetics and quantitative  
532 genetics refer to. In particular, the quantitative genetic “small shifts” view of  
533 adaptation does not talk about a stationary distribution: it does not imply that  
534 alleles will never fix over much longer time scales, due to drift and weak selection.  
535 On a technical level, the transient nature of our result means that it reflects  
536 the effects of genetic drift only during the early phase of adaptation. These  
537 early effects are crucial because they are magnified by the action of positive  
538 selection. In contrast, our result ignores drift after phenotypic adaptation has  
539 been accomplished – which is also a reason why it can be derived at all.

540 To capture the key characteristics of the adaptive architecture, we dissect the  
541 joint distribution in Eq (8) into marginal distributions of single loci. As explained  
542 at the start of the results section, these loci do not refer to a fixed genome  
543 position, but are defined *a posteriori* via their role in the adaptive process. For  
544 example, the *major locus* is defined as the locus with the largest mutant allele  
545 frequency at the end of the adaptive phase. (Since all loci have equal effects  
546 in our model, this is also the locus with the largest contribution to the adaptive  
547 response.) This is a different way to summarize the joint distribution than used in

548 some of the previous literature Chevin and Hospital (2008); Pavlidis et al. (2012);  
549 Wollstein and Stephan (2014), which rely on a gene-centered view to study the  
550 pattern at a focal locus, irrespective of its role in trait adaptation. In contrast,  
551 we use a trait-centered view, which is better suited to describe and distinguish  
552 adaptive scenarios. For example, “adaptation by sweeps” refers to a scenario  
553 where sweeps happen at some loci, rather than at a specific locus. This point is  
554 further discussed in Appendix A.5, where we also display marginal distributions  
555 of Eq (8) for fixed loci.

### 556 **The role of the background mutation rate**

557 Our results show that the qualitative pattern of polygenic adaptation is predicted  
558 by a single compound parameter: the background mutation rate  $\Theta_{bg}$  (see Eqs (10),(13),(15)),  
559 i.e., the population mutation rate for the background of a focal locus within the  
560 trait basis. For a large basis,  $\Theta_{bg}$  is closely related to the trait mutation rate.  
561 We can understand the key role of this parameter as follows. As detailed in  
562 the Section 3.4, the early stochastic phase of adaptation is governed by two  
563 processes: New successful mutations (destined for establishment) enter the population  
564 at rate  $\Theta_l s_b$  per locus (where  $\Theta_l$  is the locus mutation rate and  $s_b$  the selection  
565 coefficient), while existing mutants spread with an exponential rate  $s_b$ . Consider  
566 the locus that carries the first successful mutant. For  $\Theta_{bg} < 1$ , the expected  
567 spread from this first mutant exceeds the creation of new mutant lineages at all  
568 other loci. Therefore, the locus will likely maintain its lead, with an exponentially  
569 growing gap to the second largest locus. Vice versa, for  $\Theta_{bg} > 1$ , most likely one  
570 of the competing loci will catch up. We can thus think of  $\Theta_{bg}$  as a measure of  
571 competition experienced by the major locus due to adaptation at redundant loci  
572 in its genetic background. The argument does not depend on the strength of  
573 selection, which affects both rates in the same way. The same can be shown for  
574 adaptation from standing genetic variation at mutation-selection-drift balance. As

575 a consequence of low mutant frequencies during the stochastic phase, the result  
576 is also independent of interaction effects due to epistasis or linkage.

577 Since the order of loci is not affected by the deterministic phase of the adaptive  
578 process,  $\Theta_{bg}$  maintains its key role for the adaptive architecture. In the joint  
579 frequency distribution, Eq (5) and Eq (8), it governs the singular behavior of  
580 the marginal distribution at the major locus. For  $\Theta_{bg} < 1$ , this distribution has a  
581 singularity at the maximum of its range. Adaptation is therefore dominated by the  
582 major locus, leading to heterogeneous architectures. For  $\Theta_{bg} \lesssim 0.1$ , adaptation  
583 occurs almost always due to a completed sweep at this locus. For  $\Theta_{bg} > 1$ , in  
584 contrast, no single dominating locus exists: adaptation is collective and supported  
585 by multiple loci. For a polygenic trait with  $\Theta_{bg} \gtrsim 100$ , we obtain homogeneous  
586 small shifts at many loci, as predicted by quantitative genetics.

587 The result also shows that the adaptive scenario does not depend directly on  
588 the number of loci in the genetic basis of the trait, but rather on their combined  
589 mutation rate (the mutational target size, *sensu* Pritchard et al. (2010)). For  
590 redundant loci and fixed  $\Theta_{bg}$ , the predicted architecture at the loci with the largest  
591 contribution to the adaptive response is almost independent of the number of loci,  
592 see Fig 4. Qualitatively, the same still holds true when the assumption of complete  
593 redundancy is dropped (Fig 5). In this case, only loci in the genetic background  
594 that are not required to reach the new trait optimum, but offer redundant routes  
595 for adaptation, are included in  $\Theta_{bg}$ . Note that the same reasoning holds for  
596 a quantitative trait that is composed of several modules of mutually redundant  
597 genes, but where interactions among genes in different modules can be ignored.  
598 In this case, the adaptive architecture for each module depends only on the  
599 module-specific  $\Theta_{bg}$ , but not on the mutation rates at genes in the basis of the  
600 trait outside of the module.

## 601 **Polygenic adaptation and soft sweeps**

602 In our analysis of polygenic adaptation, we have not studied the probability that  
603 adaptation at single loci could involve more than a single mutational origin and  
604 thus produces a so-called *soft selective sweep from recurrent mutation*. As explained  
605 in Pennings and Hermisson (2006); Hermisson and Pennings (2017), however,  
606 the answer is simple and only depends on the locus mutation rate – independently  
607 of adaptation at other loci. Soft sweeps become relevant for  $\Theta_l \gtrsim 0.1$ . For  
608 much larger values  $\Theta_l \gg 1$ , they become “super-soft” in the sense that single  
609 sweep haplotypes do not reach high frequencies because there are so many  
610 independent origins of the mutant allele. The role of  $\Theta_{bg}$  for polygenic adaptation  
611 is essentially parallel to the one of  $\Theta_l$  for soft sweeps. In both cases, the population  
612 mutation rate is the only relevant parameter, with a lower threshold of  $\Theta \sim 0.1$  for a  
613 signal involving multiple alleles and much higher values for a “super-soft” scenario  
614 with only subtle frequency shifts. Nevertheless, the mathematical methods to  
615 analyze both cases are different, essentially because the polygenic scenario does  
616 not lend itself to a coalescent approach.

## 617 **5.2 Alternative approaches to polygenic adaptation**

618 The theme of “competition of a single locus with its background” relates to previous  
619 findings by Chevin and Hospital (2008) Chevin and Hospital (2008) in one of the  
620 first studies to address polygenic footprints. These authors rely on a deterministic  
621 model to describe the adaptive trajectory at a single target QTL in the presence  
622 of background variation. The background is modeled as a normal distribution with  
623 a mean that can respond to selection, but with constant variance. Obviously, a  
624 drift-related parameter, such as  $\Theta_{bg}$ , has no place in such a framework. Still, there  
625 are several correspondences to our result on a qualitative level. Specifically, a  
626 sweep at the focal locus is prohibited under two conditions. First, the background



627 variation (generated by recurrent mutation in our model, constant in Chevin and  
628 Hospital (2008)) is large. Second, the fitness function must exhibit strong negative  
629 epistasis that allows for alternative ways to reach the trait optimum – and thus  
630 produces redundancy (Gaussian stabilizing selection in Chevin and Hospital (2008)).  
631 Finally, while the adaptive trajectory depends on the *shape* of the fitness function,  
632 Chevin and Hospital note that it does not depend on the *strength* of selection on  
633 the trait, as also found for our model.

634 A major difference of the approach used in Chevin and Hospital (2008) is the  
635 gene-centered view that is applied there. Consider a scenario where the genetic  
636 background “wins” against the focal QTL and precludes it from sweeping. For  
637 a generic polygenic trait (and for our model) this still leaves the possibility of a  
638 sweep at one of the background loci. However, this is not possible in Chevin  
639 and Hospital (2008), where all background loci are summarized as a sea of  
640 small-effect loci with constant genetic variance.

641 This constraint is avoided in the approach by deVladar and Barton de Vladar  
642 and Barton (2014) and Jain and Stephan Jain and Stephan (2017), who study  
643 an additive quantitative trait under stabilizing selection with binary loci (see also  
644 Jain and Devi (2018) for an extension to adaptation to a moving optimum). These  
645 models allow for different locus effects, but ignore genetic drift. Before the environmental  
646 change, all allele frequencies are assumed to be in mutation-selection balance,  
647 with equilibrium values derived in de Vladar and Barton (2014). At the environmental  
648 change, the trait optimum jumps to a new value and alleles at all loci respond  
649 by large or small changes in the allele frequencies. Overall, de Vladar and  
650 Barton (2014) and Jain and Stephan (2017) predict adaptation by small frequency  
651 shifts in large parts of the biological parameter space. In particular, sweeps are  
652 prevented in these models if most loci have a small effect and are therefore  
653 under weak selection prior to the environmental change. This contrasts to  
654 our model, where the predicted architecture of adaptation is independent of the

655 selection strength. The reason for this difference is that effects of drift on the  
656 starting allele frequencies are neglected in the deterministic models. Indeed, loci  
657 under weak selection start out from frequency  $x_0 = 0.5$  de Vladar and Barton  
658 (2014). In finite populations, however, almost all of these alleles start from very  
659 low (or very high) frequencies – unless the population mutation parameter is  
660 large (many alleles at intermediate frequencies at competing background loci are  
661 expected only if  $\Theta_{bg} \gg 1$ , in accordance with our criterion for *shifts*). To test this  
662 further, we have analyzed our model for the case of starting allele frequencies  
663 set to the deterministic values of mutation-selection balance,  $\mu/s_d$ . Indeed, we  
664 observe adaptation due to small frequency shifts in a much larger parameter  
665 range (Appendix A.2).

666 Generally, adaptation by sweeps in a polygenic model requires a mechanism  
667 to create heterogeneity among loci. This mechanism is entirely different in both  
668 modeling frameworks. While heterogeneity is (only) produced by unequal locus  
669 effects for the deterministic quantitative trait, it is (solely) due to genetic drift for  
670 the redundant trait model. Since both approaches ignore one of these factors,  
671 both results should rather underestimate the prevalence of sweeps.

672 Both drift and unequal locus effects are included in the simulation studies by  
673 Pavlidis et al (2012) Pavlidis et al. (2012) and Wollstein and Stephan (2014)  
674 Wollstein and Stephan (2014). These authors assess patterns of adaptation  
675 for a quantitative trait under stabilizing selection with up to eight diploid loci.  
676 However, due to differences in concepts and definitions there are few comparable  
677 results. In contrast to Jain and Stephan (2017) and to our approach, they study  
678 long-term adaptation (they simulate  $N_e$  generations). In Pavlidis et al. (2012);  
679 Wollstein and Stephan (2014), *sweeps* are defined as fixation of the mutant  
680 allele at a focal locus, whereas *frequency shifts* correspond to long-term stable  
681 polymorphic equilibria Wollstein and Stephan (2014). With this definition, a *shift*  
682 scenario is no longer a transient pattern, but depends entirely on the existence

683 (and range of attraction) of polymorphic equilibria. A polymorphic outcome is  
684 likely for a two-locus model with full symmetry, where the double heterozygote  
685 has the highest fitness. For more than two loci, the probability of shifts *decreases*  
686 (because polymorphic equilibria become less likely, see Bürger and Gimelfarb  
687 (1999)). However, also the probability of a sweep decreases. This is largely due  
688 to the gene-centered view in Pavlidis et al. (2012), where potential sweeps at  
689 background loci are not recorded (see also Appendix A.5).

### 690 **5.3 Scope of the model and the analytical approach**

691 We have described scenarios of adaptation for a simple model of a polygenic  
692 trait. This model allows for an arbitrary number of loci with variable mutation  
693 rates, haploids and diploids, linkage, time-dependent selection, new mutations  
694 and standing genetic variation, and alternative starting conditions for the mutant  
695 alleles. Its genetic architecture, however, is strongly restricted by our assumption  
696 of (full or relaxed) redundancy among loci. In the haploid, fully redundant version,  
697 the phenotype is binary and only allows for two states, *ancestral wild-type* and  
698 *mutant*. Biologically, this may be thought of as a simple model for traits like  
699 pathogen or antibiotic resistance, body color, or the ability to use a certain substrate  
700 Coffman et al. (2005); Novembre and Han (2012).

701 Our main motivation, however, has been to construct a minimal model with  
702 a polygenic architecture that allows for both sweep and shifts scenarios – and  
703 for comprehensive analytical treatment. One may wonder how our methods and  
704 results generalize if we move beyond our model assumptions.

705 Key to our analytical method is the dissection of the adaptive process into a  
706 stochastic phase that explains the origin and establishment of beneficial variants  
707 and a deterministic phase that describes the allele frequency changes of the  
708 established mutant copies. This framework can be applied to a much broader  
709 class of models. Indeed, in many cases, the fate of beneficial alleles, establishment

710 or loss, is decided while these alleles are rare. Excluding complex scenarios  
711 such as passage through a fitness valley, the initial stochastic phase is relatively  
712 insensitive to interactions via epistasis or linkage. We can therefore describe the  
713 dynamics of traits with a different architecture (e.g. an additive quantitative trait  
714 with equal-effect loci under stabilizing selection) within the same framework by  
715 coupling the same stochastic dynamics to a different set of differential equations  
716 describing the dynamics during the deterministic phase.

717 This is important because, as described above, the key *qualitative* results to  
718 distinguish broad categories of adaptive scenarios are due to the initial stochastic  
719 phase. This holds true, in particular, for the role of the background mutation rate  
720  $\Theta_{bg}$ . We therefore expect that these results generalize beyond our basic model.  
721 Indeed, we have already seen this for our model extensions to include diploids,  
722 linkage, and relaxed redundancy. Vice-versa, we have seen that other factors,  
723 such as alternative starting conditions for the mutant alleles, directly affect the  
724 early stochastic phase and lead to larger changes in the results. As shown in  
725 Appendix A.2, however, they can be captured by an appropriate extension of the  
726 stochastic Yule process framework.

727 Several factors of biological importance are not covered by our current approach.  
728 Most importantly, this includes loci with different effect sizes and spatial population  
729 structure. Both require a further extension of our framework for the early stochastic  
730 phase of adaptation. While variable locus effects (both directly on the trait or  
731 on fitness due to pleiotropy) are expected to enhance the heterogeneity in the  
732 adaptive response among loci, the opposite is true for spatial structure, as further  
733 discussed below.

## 734 **5.4 When to expect sweeps or shifts**

735 Although our assumptions on the genetic architecture of the trait (complete redundancy  
736 and equal loci) are favorable for a collective, shift-type adaptation scenario, we

737 observe large changes in mutant allele frequencies (completed or partial sweeps)  
738 for major parts of the parameter range. A homogeneous pattern of *subtle frequency*  
739 *shifts* at many loci is only observed for large mutation rates. This contrasts  
740 with experience gained from breeding and modern findings from genome-wide  
741 association studies, which are strongly suggestive of an important role for small  
742 shifts with contributions from very many loci (reviewed in Falconer et al. (1996);  
743 Barton and Keightley (2002); Hill (2014); Visscher et al. (2017); Csilléry et al.  
744 (2018), see Hancock et al. (2010); Laporte et al. (2016); Zan and Carlborg (2018)  
745 for recent empirical examples). For traits such as human height, there has even  
746 been a case made for *omnigenic* adaptation Boyle et al. (2017), setting up a  
747 “mechanistic narrative” for Fisher’s (conceptual) infinitesimal model. Clearly, body  
748 height may be an extreme case and the adaptive scenario will strongly depend on  
749 the type of trait under consideration. Still, the question arises whether and how  
750 wide-spread shift-type adaptation can be reconciled with our predictions. We will  
751 first discuss this question within the scope of our model and then turn to factors  
752 beyond our model assumptions.

### 753 **The size of the background mutation rate**

754 The decisive parameter to predict the adaptive scenario in our model, the background  
755 mutation rate, is not easily amenable to measurement.  $\Theta_{bg} = (L-1)\Theta_l$  compounds  
756 two factors, the locus mutation parameter  $\Theta_l$  and the number of loci  $L$ , which are  
757 both complex themselves and require interpretation. To assess the plausibility of  
758 values of the order of  $\Theta_{bg} \gtrsim 100$ , required for homogeneous polygenic shifts in  
759 our model, we consider both factors separately.

760 Large locus mutation rates  $\Theta_l = 4N_e\mu$  (for diploids,  $2N_e\mu$  for haploids) are  
761 possible if either the allelic mutation rate  $\mu$  or the effective population size  $N_e$   
762 is large. Both cases are discussed in detail (for the case of soft sweeps) in  
763 Hermisson and Pennings (2017). Basically,  $\mu$  can be large if the mutational target

764 *at the locus* is large. Examples are loss-of-function mutations or cis-regulatory  
765 mutations.  $N_e$  is the *short-term effective population size* Pennings and Hermisson  
766 (2006); Karasov et al. (2010); Barton (2010) during the stochastic phase of adaptation.  
767 This *short-term* size is unaffected by demographic events, such as bottlenecks,  
768 prior to adaptation and is therefore often larger than the *long-term* effective size  
769 that is estimated from nucleotide diversity. (Strong changes in population size  
770 *during* the adaptive period can have more subtle effects Wilson et al. (2014).)  
771 For recent adaptations due to gain-of-function mutations, plausible values are  
772  $\Theta_l \lesssim 0.1$  for *Drosophila* and  $\Theta_l \lesssim 0.01$  for humans Hermisson and Pennings  
773 (2017).

774 If 10 000 loci or more contribute to the basis of a polygenic trait Boyle et al.  
775 (2017), large values of  $\Theta_{bg}$  could, in principle, easily be obtained. However,  
776 the parameter  $L$  in our model counts only loci that actually can respond to the  
777 selection pressure: mutant alleles must change the trait in the right direction  
778 and should not be constrained by pleiotropic effects. Omnigenic genetics, in  
779 particular, also implies ubiquitous pleiotropy and so the size of the basis *that*  
780 *is potentially available for adaptation* is probably strongly restricted. For a given  
781 trait, the number of available loci  $L$  may well differ, depending on the selection  
782 pressure and pleiotropic constraints. Furthermore, our results for the model with  
783 relaxed redundancy show that  $\Theta_{bg}$  only accounts for loci that are truly redundant  
784 and offer alternative routes to the optimal phenotype. With this in mind, values  
785 of  $L$  in the hundreds or thousands (required for  $\Theta_{bg} \geq 100$ ) seem to be quite  
786 large. While some highly polygenic traits such as body size could still fulfill this  
787 condition, this appears questionable for the generic case.

## 788 **Balancing selection and spatial structure**

789 In our model, characteristic patterns in the adaptive architecture result from heterogeneities  
790 among loci that are created by mutation and drift during the initial stochastic

791 phase of adaptation. As initial condition, we have mostly assumed that mutant  
792 alleles segregate in the population in the balance of mutation, purifying selection  
793 and genetic drift. Since this typically results in a broad allele frequency distribution  
794 (unless mutation is very strong), it favors heterogeneity among loci and thus  
795 adaptation by (partial) sweeps. However, even after decades of research, the  
796 mechanisms to maintain genetic variation in natural populations remain elusive  
797 Barton and Keightley (2002). As discussed in Appendix A.2, more homogeneous  
798 starting conditions for the mutant alleles can be strongly favorable of a shift scenario.  
799 Such conditions can be created either by balancing selection or by neutral population  
800 structure.

801 Balancing selection (due to overdominance or negative frequency dependence)  
802 typically maintains genetic variation at intermediate frequencies. If a major part  
803 of the genetic variance for the trait is due to balancing selection, adaptation could  
804 naturally occur by small shifts. However, the flexibility of alleles at single loci,  
805 and thus the potential for smaller or larger shifts, will depend on the strength of  
806 the fitness trade-off (e.g. due to pleiotropy) at each locus. If these trade-offs  
807 are heterogeneous, the adaptive architecture will reflect this. Also, adaptation  
808 against a trade-off necessarily involves a fitness cost. Therefore, if the trait can  
809 also adapt at loci that are free of a trade-off, these will be preferred, possibly  
810 leading to sweeps.

811 As discussed in a series of papers by Ralph and Coop (2010, 2015), spatial population  
812 structure is a potent force to increase the number of alternative alleles that contribute  
813 to the adaptive response. If adaptation proceeds independently, but in parallel, in  
814 spatially separated subpopulations, different alleles may be picked up in different  
815 regions. Depending on details of the migration pattern Paulose et al. (2018), we  
816 then expect architectures that are globally polygenic with small shifts, but locally  
817 still show sweeps or dominating variants.

818 Furthermore, population structure and gene flow *before* the start of the selective

819 phase can have a strong effect on the starting frequencies. In particular, if the  
820 base population is admixed, mutant alleles could often start from intermediate  
821 frequencies and naturally produce small shifts. This applies, in particular, to  
822 adaptation in modern human populations, which have experienced major admixture  
823 events in their history Lazaridis et al. (2016); Pickrell and Reich (2014) and only  
824 show few clear signals of selective sweeps Pritchard et al. (2010).

825 Finally, gene flow and drift will continue to change the architecture of adaptation  
826 after the rapid adaptive phase that has been our focus here. This can work in  
827 both directions. On the one hand, subsequent gene flow can erase any *local*  
828 sweep signals by mixing variants that have been picked up in different regions  
829 Ralph and Coop (2010, 2015). On the other hand, local adaptation, in particular,  
830 may favor adaptation by large-effect alleles at few loci, favoring sweeps over  
831 longer time-scales. Indeed, as argued by Yeaman Yeaman (2015), initial rapid  
832 adaptation due to small shifts at many alleles of mostly small effect may be  
833 followed by a phase of allelic turnover, during which alleles with small effect  
834 are swamped and few large-effect alleles eventually take over. This type of  
835 allele sorting over longer time-scales is also observed in simulations studies for a  
836 quantitative trait under stabilizing selection that adapt to a new optimum after an  
837 environmental change Franssen et al. (2017); Jain and Stephan (2017).

### 838 **Between sweeps and shifts: adaptation by partial sweeps**

839 Previous research has almost entirely focused on either of the two extreme scenarios  
840 for adaptation: sweeps in a single-locus setting or (infinitesimal) shifts in the  
841 tradition of Fisher's infinitesimal model. This leaves considerable room for intermediate  
842 patterns. Our results for the redundant trait model show that such transitional  
843 patterns should be expected in a large and biologically relevant parameter range  
844 (values of  $\Theta_{bg}$  between 0.1 and 100). Patterns between sweeps and shifts are  
845 *polygenic* in the sense that they result from the *concerted* change in the allele



846 frequency at multiple loci. They can only be understood in the context of interactions  
847 among these loci. However, they usually do not show subtle shifts, but much  
848 larger changes (partial sweeps) at several loci. If adaptation occurs from mutation-selection-drift  
849 balance, the polygenic patterns are typically strongly heterogeneous, even across  
850 loci with identical effects on the trait. Such patterns may be difficult to detect  
851 with classical sweep scans, in particular if partial sweeps are "soft" because they  
852 originate from standing genetic variation or involve multiple mutational origins.  
853 However, they should be visible in time-series data and may also leave detectable  
854 signals in local haplotype blocks.

855       Indeed there is empirical evidence for partial sweeps from time series data in  
856 experimental *evolve and resequence* experiments on recombining species such  
857 as fruit flies. For example, Burke *et al.* Burke et al. (2010) observe predominantly  
858 partial sweeps (from SGV) in their long-term selection experiments with *Drosophila*  
859 *melanogaster* for accelerated development – a rather unspecific trait with a presumably  
860 large genomic basis. A similar pattern of “plateauing”, where allele frequencies at  
861 several loci increase quickly over several generations, but then stop at intermediate  
862 levels, was recently observed by Barghi and collaborators Barghi et al. (2018) for  
863 adaptation of 10 *Drosophila simulans* replicates to a hot temperature environment.  
864 Complementing the genotypic time-series data with measurements of several  
865 phenotypes, these authors found convergent evolution for several high-level traits  
866 (such as fecundity and metabolic rate), indicating that rapid phenotypic adaptation  
867 had reached a new optimum. This high-level convergence contrasts a strong  
868 heterogeneity in the adaptation response among loci and also between replicates  
869 Barghi et al. (2018). Based on their data, the authors reject both a selective  
870 sweep model and adaptation by subtle shifts. Instead, the observed patterns  
871 are most consistent with the intermediate adaptive scenario in our framework,  
872 featuring heterogeneous partial sweeps at interacting loci with a high level of  
873 genetic redundancy.

## 874 **References**

- 875 Barghi, N., Tobler, R., Nolte, V., Jaksic, A. M., Mallard, F., Otte, K., Dolezal, M., Taus, T.,  
876 Kofler, R., and Schloetterer, C. (2018). Polygenic adaptation fuels genetic redundancy  
877 in drosophila. *bioRxiv*, page 332122.
- 878 Barton, N. (1998). The effect of hitch-hiking on neutral genealogies. *Genetics Research*,  
879 72(2):123–133.
- 880 Barton, N. (2010). Understanding adaptation in large populations. *PLoS genetics*,  
881 6(6):e1000987.
- 882 Barton, N., Etheridge, A., and Véber, A. (2017). The infinitesimal model: Definition,  
883 derivation, and implications. *Theoretical population biology*, 118:50–73.
- 884 Barton, N. and Keightley, P. D. (2002). Multifactorial genetics: understanding quantitative  
885 genetic variation. *Nature Reviews Genetics*, 3(1):11.
- 886 Berg, J. J. and Coop, G. (2014). A population genetic signal of polygenic adaptation.  
887 *PLoS genetics*, 10(8):e1004412.
- 888 Berg, J. J., Harpak, A., Sinnott-Armstrong, N., Joergensen, A. M., Mostafavi, H., Field,  
889 Y., Boyle, E. A., Zhang, X., Racimo, F., Pritchard, J. K., and Coop, G. (2018). Reduced  
890 signal for polygenic adaptation of height in uk biobank. *bioRxiv*.
- 891 Boyle, E. A., Li, Y. I., and Pritchard, J. K. (2017). An expanded view of complex traits:  
892 from polygenic to omnigenic. *Cell*, 169(7):1177–1186.
- 893 Bürger, R. (2000). *The mathematical theory of selection, recombination, and mutation*.  
894 Wiley.
- 895 Bürger, R. and Gimelfarb, A. (1999). Genetic variation maintained in multilocus models  
896 of additive quantitative traits under stabilizing selection. *Genetics*, 152(2):807–820.
- 897 Bürger, R. and Lynch, M. (1995). Evolution and extinction in a changing environment: a  
898 quantitative-genetic analysis. *Evolution*, 49(1):151–163.

- 899 Burke, M., Dunham, J., Shahrestani, P., Thornton, K., Rose, M., and Long, A. (2010).  
900 Genome-wide analysis of a long-term evolution experiment with drosophila. *Nature*,  
901 467(7315):587–590.
- 902 Chevin, L.-M. and Hospital, F. (2008). Selective sweep at a quantitative trait locus in the  
903 presence of background genetic variation. *Genetics*.
- 904 Coffman, C. J., Doerge, R. W., Simonsen, K. L., Nichols, K. M., Duarte, C., Wolfinger,  
905 R. D., and McIntyre, L. (2005). Model selection in binary trait locus mapping. *Genetics*.
- 906 Csilléry, K., Rodríguez-Verdugo, A., Rellstab, C., and Guillaume, F. (2018). Detecting the  
907 genomic signal of polygenic adaptation and the role of epistasis in evolution. *Molecular*  
908 *ecology*.
- 909 de Vladar, H. P. and Barton, N. (2014). Stability and response of polygenic traits to  
910 stabilizing selection and mutation. *Genetics*, 197(2):749–767.
- 911 Etheridge, A., Pfaffelhuber, P., Wakolbinger, A., et al. (2006). An approximate sampling  
912 formula under genetic hitchhiking. *The Annals of Applied Probability*, 16(2):685–729.
- 913 Falconer, D., Mackay, T., and Bulmer, M. (1996). Introduction to quantitative genetics.  
914 *Genetical Research*, 68(2):183.
- 915 Field, Y., Boyle, E. A., Telis, N., Gao, Z., Gaulton, K. J., Golan, D., Yengo, L., Rocheleau,  
916 G., Froguel, P., McCarthy, M. I., et al. (2016). Detection of human adaptation during  
917 the past 2000 years. *Science*, page aag0776.
- 918 Fisher, R. A. (1918). The correlation between relatives on the supposition of mendelian  
919 inheritance.
- 920 Franssen, S., Kofler, R., and Schlötterer, C. (2017). Uncovering the genetic signature of  
921 quantitative trait evolution with replicated time series data. *Heredity*, 118(1):42.
- 922 Geritz, S. A., Mesze, G., Metz, J. A., et al. (1998). Evolutionarily singular strategies  
923 and the adaptive growth and branching of the evolutionary tree. *Evolutionary ecology*,  
924 12(1):35–57.

- 925 Griffiths, R. and Tavaré, S. (1998). The age of a mutation in a general coalescent tree.  
926 *Stochastic Models*, 14(1-2):273–295.
- 927 Hancock, A. M., Alkorta-Aranburu, G., Witonsky, D. B., and Di Rienzo, A. (2010).  
928 Adaptations to new environments in humans: the role of subtle allele frequency shifts.  
929 *Philosophical Transactions of the Royal Society of London B: Biological Sciences*,  
930 365(1552):2459–2468.
- 931 Hermisson, J. and Pennings, P. S. (2005). Soft sweeps: molecular population genetics of  
932 adaptation from standing genetic variation. *Genetics*, 169(4):2335–2352.
- 933 Hermisson, J. and Pennings, P. S. (2017). Soft sweeps and beyond: understanding the  
934 patterns and probabilities of selection footprints under rapid adaptation. *Methods in*  
935 *Ecology and Evolution*, 8(6):700–716.
- 936 Hermisson, J. and Pfaffelhuber, P. (2008). The pattern of genetic hitchhiking under  
937 recurrent mutation. *Electronic Journal of Probability*, 13:2069–2106.
- 938 Hill, W. G. (2014). Applications of population genetics to animal breeding, from wright,  
939 fisher and lush to genomic prediction. *Genetics*, 196(1):1–16.
- 940 Hoppe, F. M. (1984). Pólya-like urns and the ewens' sampling formula. *Journal of*  
941 *Mathematical Biology*, 20(1):91–94.
- 942 Inc., W. R. Mathematica, Version 11.3. Champaign, IL, 2018.
- 943 Jain, K. and Devi, A. (2018). Polygenic adaptation in changing environments. *arXiv*  
944 *preprint arXiv:1806.03454*.
- 945 Jain, K. and Stephan, W. (2015). Response of polygenic traits under stabilizing selection  
946 and mutation when loci have unequal effects. *G3: Genes, Genomes, Genetics*,  
947 5(6):1065–1074.
- 948 Jain, K. and Stephan, W. (2017). Rapid adaptation of a polygenic trait after a sudden  
949 environmental shift. *Genetics*, 206(1):389–406.

950 Kaplan, N. L., Hudson, R., and Langley, C. (1989). The "hitchhiking effect" revisited.  
951 *Genetics*, 123(4):887–899.

952 Karasov, T., Messer, P. W., and Petrov, D. A. (2010). Evidence that adaptation in  
953 *Drosophila* is not limited by mutation at single sites. *PLoS genetics*, 6(6):e1000924.

954 Kryazhimskiy, S., Rice, D. P., Jerison, E. R., and Desai, M. M. (2014). Global  
955 epistasis makes adaptation predictable despite sequence-level stochasticity. *Science*,  
956 344(6191):1519–1522.

957 Lande, R. (1983). The response to selection on major and minor mutations affecting a  
958 metrical trait. *Heredity*, 50(1):47.

959 Laporte, M., Pavey, S. A., Rougeux, C., Pierron, F., Lauzent, M., Budzinski, H., Labadie,  
960 P., Geneste, E., Couture, P., Baudrimont, M., et al. (2016). Rad sequencing reveals  
961 within-generation polygenic selection in response to anthropogenic organic and metal  
962 contamination in north atlantic eels. *Molecular ecology*, 25(1):219–237.

963 Lazaridis, I., Nadel, D., Rollefson, G., Merrett, D. C., Rohland, N., Mallick, S., Fernandes,  
964 D., Novak, M., Gamarra, B., Sirak, K., et al. (2016). Genomic insights into the origin of  
965 farming in the ancient near east. *Nature*, 536(7617):419.

966 Matuszewski, S., Hermisson, J., and Kopp, M. (2015). Catch me if you can: adaptation  
967 from standing genetic variation to a moving phenotypic optimum. *Genetics*, pages  
968 genetics–115.

969 Maynard-Smith, J. and Haigh, J. (1974). The hitch-hiking effect of a favourable gene.  
970 *Genetics Research*, 23(1):23–35.

971 Messer, P. W., Ellner, S. P., and Hairston Jr, N. G. (2016). Can population genetics adapt  
972 to rapid evolution? *Trends in Genetics*, 32(7):408–418.

973 Novembre, J. and Han, E. (2012). Human population structure and the adaptive response  
974 to pathogen-induced selection pressures. *Phil. Trans. R. Soc. B*, 367(1590):878–886.

- 975 Orr, H. (2005). The genetic theory of adaptation: a brief history. *Nature Reviews Genetics*,  
976 6(2):119–127.
- 977 Orr, H. A. and Betancourt, A. J. (2001). Haldane’s sieve and adaptation from the standing  
978 genetic variation. *Genetics*, 157(2):875–884.
- 979 Paulose, J., Hermisson, J., and Hallatschek, O. (2018). Spatial soft sweeps: patterns of  
980 adaptation in populations with long-range dispersal. *bioRxiv*, page 299453.
- 981 Pavlidis, P., Metzler, D., and Stephan, W. (2012). Selective sweeps in multilocus models  
982 of quantitative traits. *Genetics*, 192(1):225–239.
- 983 Pennings, P. and Hermisson, J. (2006). Soft sweeps ii—molecular population genetics  
984 of adaptation from recurrent mutation or migration. *Molecular biology and evolution*,  
985 23(5):1076–1084.
- 986 Pickrell, J. K. and Reich, D. (2014). Toward a new history and geography of human genes  
987 informed by ancient dna. *Trends in Genetics*, 30(9):377–389.
- 988 Pritchard, J., Pickrell, J., and Coop, G. (2010). The genetics of human adaptation: hard  
989 sweeps, soft sweeps, and polygenic adaptation. *Current biology*, 20(4):R208–R215.
- 990 Pritchard, J. K. and Di Rienzo, A. (2010). Adaptation—not by sweeps alone. *Nature*  
991 *Reviews Genetics*, 11(10):665.
- 992 Ralph, P. L. and Coop, G. (2010). Parallel adaptation: one or many waves of advance of  
993 an advantageous allele? *Genetics*.
- 994 Ralph, P. L. and Coop, G. (2015). The role of standing variation in geographic convergent  
995 adaptation. *The American Naturalist*, 186(S1):S5–S23.
- 996 Sohail, M., Maier, R. M., Ganna, A., Bloemendal, A., Martin, A. R., Turchin, M. C., Chiang,  
997 C. W. K., Hirschhorn, J. N., Daly, M., Patterson, N., Neale, B., Mathieson, I., Reich,  
998 D., and Sunyaev, S. R. (2018). Signals of polygenic adaptation on height have been  
999 overestimated due to uncorrected population structure in genome-wide association  
1000 studies. *bioRxiv*.

- 1001 Stephan, W. (2016). Signatures of positive selection: from selective sweeps at individual  
1002 loci to subtle allele frequency changes in polygenic adaptation. *Molecular ecology*,  
1003 25(1):79–88.
- 1004 Turelli, M. and Barton, N. (1990). Dynamics of polygenic characters under selection.  
1005 *Theoretical Population Biology*, 38(1):1–57.
- 1006 Turelli, M. and Barton, N. (1994). Genetic and statistical analyses of strong selection on  
1007 polygenic traits: what, me normal? *Genetics*, 138(3):913–941.
- 1008 Visscher, P. M., Wray, N. R., Zhang, Q., Sklar, P., McCarthy, M. I., Brown, M. A., and  
1009 Yang, J. (2017). 10 years of gwas discovery: biology, function, and translation. *The*  
1010 *American Journal of Human Genetics*, 101(1):5–22.
- 1011 Wilson, B. A., Petrov, D. A., and Messer, P. W. (2014). Soft selective sweeps in complex  
1012 demographic scenarios. *Genetics*, pages genetics–114.
- 1013 Wollstein, A. and Stephan, W. (2014). Adaptive fixation in two-locus models of stabilizing  
1014 selection and genetic drift. *Genetics*, pages genetics–114.
- 1015 Wright, S. (1931). Evolution in mendelian populations. *Genetics*, 16(2):97.
- 1016 Yeaman, S. (2015). Local adaptation by alleles of small effect. *The American Naturalist*,  
1017 186(S1):S74–S89.
- 1018 Zan, Y. and Carlborg, Ö. (2018). A multilocus association analysis method integrating  
1019 phenotype and expression data reveals multiple novel associations to flowering time  
1020 variation in wild-collected arabidopsis thaliana. *Molecular ecology resources*.

## 1021 **A Supporting information**

### 1022 **A.1 Linked loci**

1023 Negative epistasis for fitness causes negative linkage disequilibrium (LD) among  
1024 the selected loci. While LD can usually be ignored as long as loci are unlinked,  
1025 this changes once recombination rates drop below the selection coefficient  $r < s_b$   
1026 (data not shown). For tight linkage  $r \rightarrow 0$ , in particular, individuals carrying  
1027 multiple mutations can no longer be formed by recombination, but require multiple  
1028 mutational hits on the same haplotype. This is unlikely while mutant allele frequencies  
1029 are low, which is when the relevant mutations of the adaptive process arise. By  
1030 the end of the adaptive phase, the excess of single-mutant haplotypes produces  
1031 strong negative LD. Nevertheless, our theory predicts that the distribution of allele  
1032 frequency ratios that emerges from the early stochastic phase of the adaptive  
1033 process is unaffected Eq.(9). This prediction is confirmed by simulations, see  
1034 Fig S.1. If anything, the match even improves for strong linkage. (Deviations for  
1035 high  $\Theta_l$  values result since the rate of recurrent mutation  $\sim \Theta_l(1-p)$  is smaller than  
1036 assumed in the Yule process approximation,  $\sim \Theta_l$ , when the mutant frequency  $p$   
1037 gets large. This affects the major locus stronger than any other locus and leads  
1038 to overshooting of the minor/major ratio seen in the Figure. The bias is reduced  
1039 for strong linkage since 95% phenotypic adaptation corresponds to smaller allele  
1040 frequencies in this case.)

1041 Fig S.2 shows the joint distribution of the major and the minor locus of a trait  
1042 with  $L = 2$  loci for different degrees of linkage. In all cases, the process is stopped  
1043 when the proportion of remaining non-mutant individuals drops below  $f_w = 0.05$ .  
1044 The results show that the linkage equilibrium assumption (red and blue lines)  
1045 provides a good approximation as long as  $r \geq s_b$ . For  $r < s_b$ , the distributions are  
1046 shifted to lower values and clear deviations become visible. The constraint on the



1047 allele frequencies at the stopping condition changes from  $(1 - p_1)(1 - p_2) = f_w$  for  
1048 linkage equilibrium to  $p_1 + p_2 = 1 - f_w$  for complete linkage. As a consequence, the  
1049 boundary between the major and minor locus distributions (red and blue) drops  
1050 from  $1 - \sqrt{f_w}$  to  $(1 - f_w)/2$ . As shown in the Mathematical Appendix, Eq (M.29), we  
1051 can derive an analytical approximation for the distributions for complete linkage  
1052  $r = 0$ . For  $L = 2$ , we obtain a modified Beta-distribution (black lines in the Figure)

$$\mathbf{P}_{f_w, \mathfrak{t}}^{\pm}[p|\Theta] = \frac{2(1 - f_w)^{-1}}{B[\Theta]} \left( \frac{p}{1 - f_w} \right)^{\Theta - 1} \left( 1 - \frac{p}{1 - f_w} \right)^{\Theta - 1} \quad (\text{S.1})$$

1053 with  $p \geq (1 - f_w)/2$  (resp.  $p \leq (1 - f_w)/2$ ) for the major (minor) locus. The  
1054 simulation results show that this prediction is accurate for  $r \ll s_b$  (deviations for  
1055  $\Theta_{bg} = 100$  are due to overshooting of the stopping condition in the last generation  
1056 of our Wright-Fisher simulations).

1057 While linkage affects the shape of the joint distribution, it does not alter its  
1058 key qualitative characteristics that distinguish adaptive scenarios. In particular,  
1059 the same conditions on  $\Theta_{bg}$  and  $\Theta_l$  apply for singularities at the boundaries of  
1060 marginal distributions. We still observe sweep-like adaptation for  $\Theta_{bg} \ll 1$ , adaptation  
1061 by small shifts for  $\Theta_{bg} \gg 1$ , and a heterogeneous pattern of partial sweeps in a  
1062 transition range of  $\Theta_{bg}$  around 1.

## 1063 **A.2 Alternative starting allele frequencies**

1064 So far we have assumed that adaptation starts from mutation-selection-drift balance.  
1065 This includes variable amounts of standing genetic variation (weak or strong  $s_d$ )  
1066 and even cases where this balance is not represented by a stable equilibrium  
1067 distribution (time-dependent selection, see the Mathematical Appendix). There  
1068 are, however, other scenarios of biological relevance. Given the right (possibly  
1069 complex) selection scheme, balancing selection can maintain mutant alleles, prior  
1070 to the environmental change, at arbitrary frequencies. The same holds true

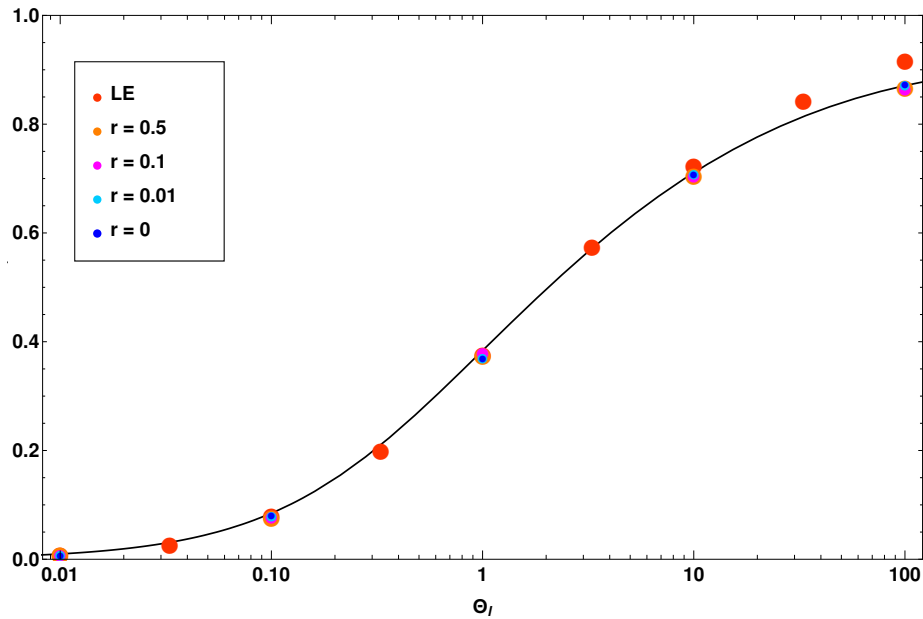


Figure S.1:  $E[x]$  for redundant fitness effects with two linked loci. Simulation results (colored dots) for the mean allele frequency ratio are plotted in dependence of the locus population mutation rate  $\Theta_l$  and compared with the analytical prediction (black line). Simulations are stopped when fitness has reached 95% of its maximum. Linkage does not change the results for the ratio of allele frequencies, despite significant build up of linkage disequilibrium with low recombination rates (data not shown). Results for 10 000 replicates standard errors  $< 0.005$  (smaller than symbols).

1071 if the base population is admixed, either due to natural processes or due to  
1072 human activity (e.g. breeding from hybrids). For these scenarios, our theoretical  
1073 formalism to describe the establishment of mutants during the stochastic phase  
1074 (Fig 2) does not apply. In this section, we describe how the formalism can be  
1075 extended to cover arbitrary starting frequencies of mutants at the onset of positive

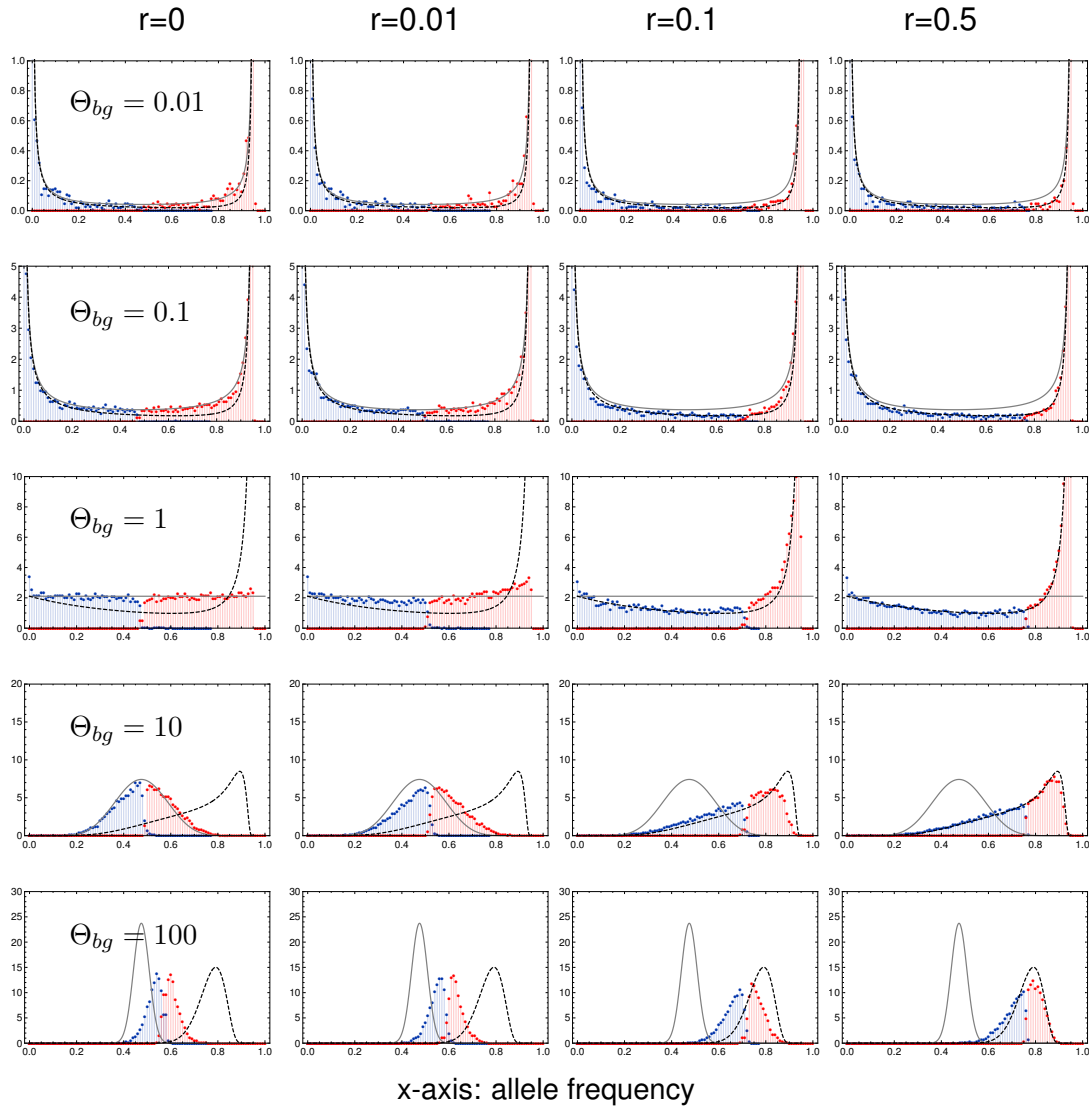


Figure S.2: **Genetic architecture of adaptation with linkage.** Marginal distributions for the major locus (red) and the minor locus (blue) of a model with  $L = 2$  loci depending on  $\Theta_{bg}$  (rows) and linkage among the loci (columns). Black lines show the analytical approximations for LE (dashed) and complete linkage (solid). For strong recombination  $r \geq s_b = 0.1$ , the deviations from the LE approximation are small. For  $r \ll s_b = 0.1$ , the approximation for complete linkage works well. Further parameters:  $-s_d = s_b = 0.1$ ,  $N_e = 10\,000$ , 10 000 replicates.

1076 selection at time  $t = 0$ .

### 1077 **Extended Yule framework**

1078 The Yule process that describes the stochastic phase of the adaptive process  
 1079 accounts for the mutant copies at all loci that are destined for establishment. In

1080 our framework so far (see the Mathematical Appendix M.2), we have started this  
1081 process with zero copies. SGV due to mutation-selection-drift balance can still  
1082 be produced by such a process if it is started at some time in the past ( $t < 0$ ).  
1083 For general starting frequencies, we can alternatively start this process at time  
1084  $t = 0$ , but with mutant copies (immortal lineages) already present. Suppose  
1085 that the mutant frequency at locus  $i$  at time  $t = 0$  is  $p_i$ , corresponding to  $N_e p_i$   
1086 mutant copies. Of these, only the  $n_i < N_e p_i$  "immortal" mutants (destined for  
1087 establishment) are included in the Yule process. Assuming an independent establishment  
1088 probability  $p_{\text{est}}$  per copy,  $n_i$  is binomially distributed with parameters  $N_e p_i$  and  $p_{\text{est}}$ .  
1089 For the limit distribution of a multi-type Yule process that is started with a non-zero  
1090 number of lines, consider that each of these initial lines can be understood as an  
1091 extra source of new immortal lines (due to birth) that is entirely equivalent to the  
1092 generation of new lineages by mutation. It is therefore appropriate to include  
1093 these lines as *extra locus mutation rate*

$$\tilde{\Theta}_i = \Theta_i + n_i = 2N_e \mu_i + n_i. \quad (\text{S.2})$$

1094 In the absence of recurrent mutation,  $\Theta_i = 0$ , this procedure reproduces the  
1095 well-know Polya urn scheme (e.g. Griffiths and Tavaré (1998); Hoppe urn: Hoppe  
1096 (1984)). Replacing  $\Theta_i$  by  $\tilde{\Theta}_i$  within our original Yule process formalism, and  
1097 averaging over the binomial distribution, leads to the desired extension to arbitrary  
1098 starting frequencies.

## 1099 **Application**

1100 Theory papers (e.g. Orr and Betancourt (2001); de Vladar and Barton (2014); Jain  
1101 and Stephan (2015, 2017)) often use a deterministic framework to describe the  
1102 frequency of alleles that segregate in a population in mutation-selection balance.  
1103 To simplify the analysis, they do not model SGV as a distribution (due to mutation,

1104 selection, and drift), but replace this distribution by its expected value (ignoring  
1105 drift). We can apply our scheme with fixed starting frequencies to this case and  
1106 thus assess the effect of genetic drift in the starting allele frequency distribution.  
1107 We assume equal loci and a starting frequency  $|\mu_l/s_d|$  for an (initially deleterious)  
1108 mutant allele with selection coefficient  $s_d$  in the mutation-selection balance. Fig S.3  
1109 shows the simulated marginal distributions of the loci with the largest contribution  
1110 to the adaptive response (compare Fig 4). We see that the type of the adaptive  
1111 architecture is again constant across rows with equal background mutation rate.  
1112 However, due to the more homogeneous starting conditions, adaptation involves  
1113 more loci and is much more shift-like. Analytical predictions following the above  
1114 scheme are shown for  $L = 2$  loci. With establishment probability  $p_{\text{est}} = 2s_b$ , the  
1115 counts  $n_1$  and  $n_2$  of "immortal" mutants at both loci are independent random draws  
1116 from a Binomial distribution with parameters  $N_e|\mu_l/s_d| = |\Theta_l/2s_d|$  and  $2s_b$ . For  
1117  $\Theta_{bg} \geq 0.1$ , we find (heuristically) that the marginal distribution for alleles starting  
1118 from mutation-selection balance closely matches the one of the fully stochastic  
1119 model with effective  $\Theta_{bg}^{\text{eff}} = \Theta_{bg}(1 + |s_b/2s_d|) = 51\Theta_{bg}$  for the parameters in the  
1120 figure (lines added in green). (Note that, from the average number of established  
1121 lines, one would assume  $\Theta_{bg}^{\text{eff}} = \Theta_{bg}(1 + |s_b/s_d|) = 101\Theta_{bg}$ . However, this does not  
1122 account for the variance in the number of immortal lines among the two loci.)

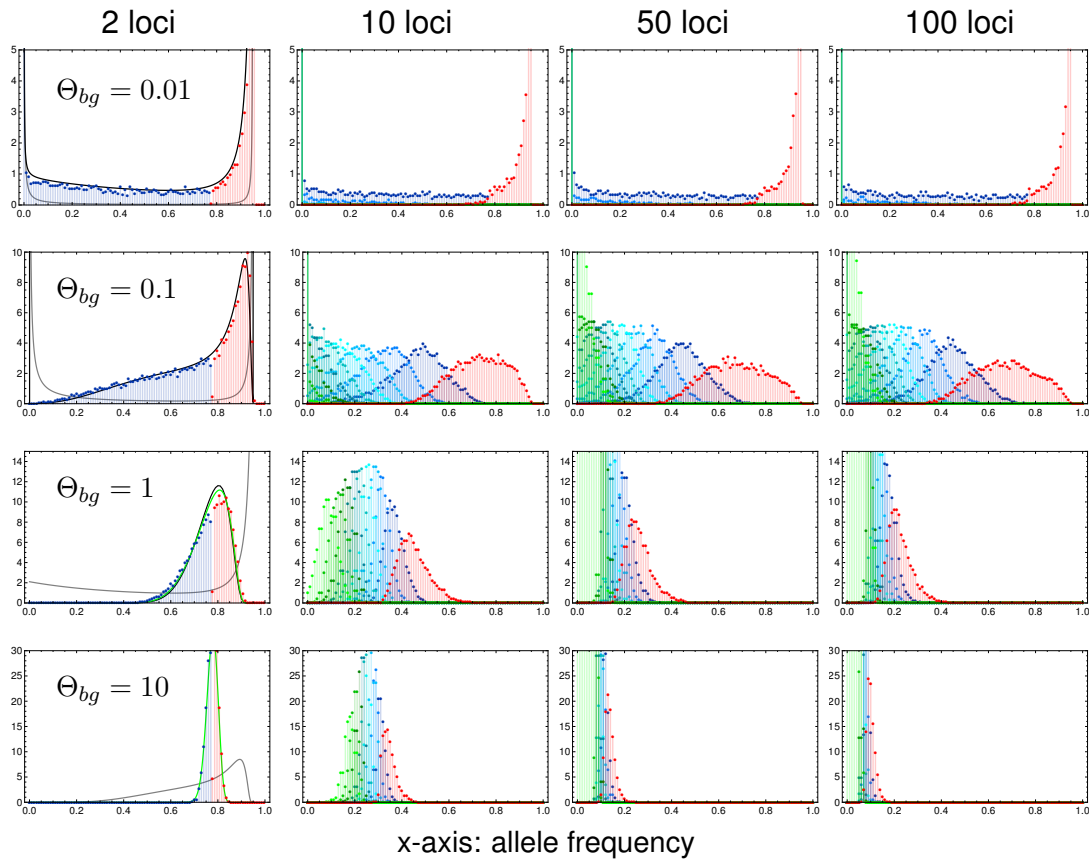


**Figure S.3: Polygenic adaptation from alternative allele starting frequencies.** The panels show the adaptive architecture when mutant alleles start from their expected value in mutation-selection balance, without drift. We distribute  $L \cdot |\Theta_l/2s_d|$  mutant copies as evenly as possible across all loci. We set  $-s_d = s_b/100 = 0.001$ . Black lines for  $L = 2$  loci show analytical predictions described in the main text (only computationally possible for  $\Theta_{bg} \leq 1$ ), green lines for  $\Theta_{bg} \geq 1$  show the heuristic prediction for  $\Theta_{bg}^{\text{eff}} = 51\Theta_{bg}$ . Finally, gray lines show the marginal distributions when adaptation occurs from mutation-selection-drift balance, compare Fig 4.

### 1123 A.3 Diploids

1124 To extend our model to diploids, we assume that a single locus that is *homozygous*  
 1125 for the mutant allele is sufficient to produce the fully functional mutant phenotype,  
 1126 while a *heterozygous* locus produces a mutant that is functional with probability  
 1127  $1 - h$ . We assume that mutants contribute independently. Thus, if  $k$  heterozygous  
 1128 loci exist, but no homozygous mutant locus, the resulting mutant phenotype will  
 1129 be functional with probability  $1 - (1 - (1 - h))^k = 1 - h^k$ . For  $L = 2$  loci, in particular,

1130 the (logarithmic) fitness of genotype  $G$  becomes

$$w(G) = \begin{cases} 0 & \text{no mutations: } G = (aabb) \\ (1-h)s & \text{1 heterozygous locus: } G = (Aabb, aaBb) \\ (1-h^2)s & \text{2 heterozygous loci: } G = (AaBb) \\ s & \geq 1 \text{ homozygous mutation: } G = (AA\dots BB) \end{cases}, \quad (\text{S.3})$$

where  $s = s_b > 0$  for  $t \geq 0$  and  $s = s_d < 0$  for  $t < 0$ . Note that  $h \in [0, 1]$  measures the dominance of the *ancestral* allele. We assume Hardy-Weinberg-linkage-equilibrium (HWLE). In this case, the marginal fitnesses of the mutant alleles are (for 2 loci),

$$w_A^* = s - (1 - p_A)(1 - p_B)[1 - p_B(1 - 2h)]hs, \quad (\text{S.4a})$$

$$w_B^* = s - (1 - p_A)(1 - p_B)[1 - p_A(1 - 2h)]hs. \quad (\text{S.4b})$$

1131 In contrast to the haploid case, the marginal fitnesses are in general *not* equal.  
 1132 There are, however, two important special cases, where our fitness scheme  
 1133 (with redundancy on the level of loci) implies equal marginal fitnesses (and thus  
 1134 redundancy on the level of alleles): either if the ancestral allele is fully recessive  
 1135 ( $h = 0$ ) or if the alleles are co-dominant ( $h = 0.5$ ). As shown in the Mathematical  
 1136 Appendix, this holds true more generally for an arbitrary number of loci.

### 1137 **Simulation results**

1138 We simulated a diploid model with two loci in HWLE according to the above  
 1139 scheme with three different levels of dominance of the ancestral allele,  $h =$   
 1140  $0.1; 0.5; \text{ and } 0.9$ . The diploid, effective population size is  $N_e$ , corresponding to  $2N_e$   
 1141 chromosomes. The mutation rate is  $\mu$  at both loci and we define the population-scaled  
 1142 mutation rate for diploids as  $\Theta_l^d = \Theta_{bg}^d = 4N_e\mu$ . Simulations are stopped when  
 1143 the percentage of remaining ancestral *haplotypes* drops below  $f_w = 0.05$ . (This

1144 condition directly corresponds to the stopping condition for haploids. Alternative  
1145 stopping conditions, such as 95% increase in mean diploid fitness are also covered  
1146 by our theoretical framework, but require a different transformation.)

1147 The results are shown in Fig S.4. We see that the haploid results fully carry  
1148 over to diploids for co-dominance ( $h = 0.5$ , middle column), where the diploid  
1149 fitness scheme implies redundancy on the level of alleles. As explained above,  
1150 the same holds true if the ancestral allele is fully recessive. Our simulations show  
1151 that the haploid result is still a good approximation for  $h = 0.1$  (left column). In  
1152 contrast, much larger deviations are obtained for recessive mutants (dominant  
1153 ancestral allele,  $h = 0.9$ , right column). In this case, the locus with the larger  
1154 mutant frequency experiences stronger selection. For  $\Theta_l \geq 0.1$ , when polymorphism  
1155 at both loci is likely, this favors the major locus relative to the minor locus, increasing  
1156 the heterogeneity in the adaptive architecture.



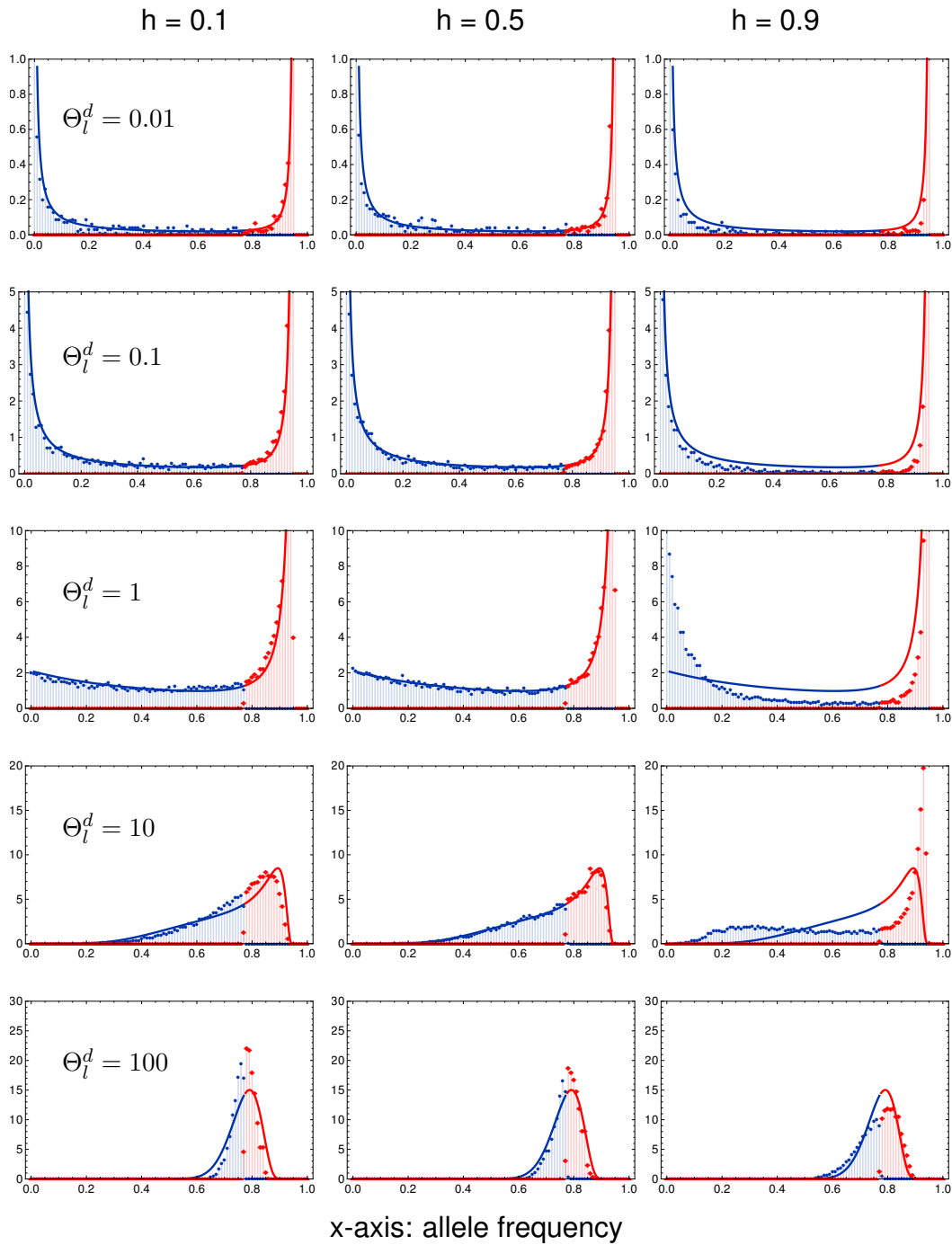


Figure S.4: **Adaptive architecture for diploids in linkage equilibrium.** Adaptation in a 2-locus model according to scheme (S.3), with recessive ( $h = 0.1$ ), codominant ( $h = 0.5$ ) or dominant ( $h = 0.9$ ) ancestral alleles. We assume Hardy-Weinberg and linkage equilibrium. Simulations are stopped when the wild type haplotypes drops below 5%. Standing genetic variation builds up for  $16N_e$  generations before the change in the environment. Selection coefficients are set to  $s_b = -s_d = 0.1$ . Solid lines show analytical predictions using the framework developed for haploids.

## 1157 **A.4 Approximations for multi-locus architectures**

1158 For tight linkage, where the joint distribution of mutant alleles is given by a Dirichlet  
1159 distribution, Mathematical Appendix Eq (M.29), lower dimensional marginal distributions  
1160 for single loci or groups of loci can easily be derived. For linkage equilibrium,  
1161 Mathematical Appendix Eq (M.20), however, the required integrals can only be  
1162 solved numerically. For  $L$  loci, an  $(L-2)$ -dim integral needs to be evaluated, which  
1163 becomes computationally unfeasible (with programs packages like *Mathematica*)  
1164 for  $L > 5$ . Nevertheless, we can derive approximations for the marginal distributions  
1165 of polygenic models with large  $L$  in many cases. To do so, we make use of a key  
1166 property of the adaptive architecture, shown in our results: The (joint) architecture  
1167 of adaptation at loci with the largest contribution to the adaptive response is  
1168 primarily a function of combined mutation rates at competing loci, such as the  
1169 background mutation rate  $\Theta_{bg}$ . Given these values, it is largely independent of the  
1170 number of loci in the genetic basis of the trait itself. We can therefore describe  
1171 the adaptive architecture of a polygenic trait with  $L$  loci by a model with  $k < L$   
1172 loci *given that* the total adaptive response is well captured by the contribution  
1173 of the top  $k$  loci. It turns out that this is typically the case for  $\Theta_{bg} < 1$ , when  
1174 the contributions from different loci are very heterogeneous. In the following, we  
1175 describe this procedure for an  $L$ -locus model with equal mutation rates  $\Theta_i = \Theta_l$   
1176 for  $1 \leq i \leq L$ .

### 1177 **Approximations using the 2-locus model**

1178 Several key properties of the  $L$ -locus architecture can already be described by  
1179 the 2-locus framework. This includes the marginal distributions at the major  
1180 locus and at the first minor locus. This requires that the mutation rate at the  
1181 minor locus of the 2-locus model matches the background mutation rate of the  
1182  $L$ -locus model. As described in the main text, this choice matches the time

1183 lag between the first origin of a mutation destined for establishment at a locus  
1184 (usually the major locus) and at a second locus (usually the first minor locus). It  
1185 also guarantees that the approximation captures the correct asymptotic shape of  
1186 the major-locus distribution at  $p = 1 - f_w$ , and of the first-minor-locus distribution  
1187 at  $p = 0$ . The choice of the mutation rate at the major locus itself is far less  
1188 important. For the approximation of the major locus distribution, we find that  
1189 setting it to the locus-mutation rate yields the best fit. We thus use a 2-locus  
1190 model with unequal mutation rates,  $P_{f_w}^{1>}[p_1|\Theta_l, \Theta_{bg}]$ , Eq (M.28a), in Fig 4. For  
1191 the marginal distribution at the first minor locus, the approximation with equal  
1192 mutation rates,  $P_{f_w}^{1<}[p_1|\Theta_{bg}, \Theta_{bg}]$ , Eq (M.28b), works slightly better. Finally, we can  
1193 also approximate the distribution at an *average* minor locus (rather than the first  
1194 minor locus) by  $P_{f_w}^{1<}[p_1|\Theta_l, \Theta_{bg}]$ .

### 1195 **Approximations using models with $k \geq 2$ loci**

1196 The approximation of higher-order minor loci requires models with a sufficiently  
1197 large genetic basis that such a locus exists at all. I.e., a  $k$ -locus model can  
1198 approximate marginal distributions up to the  $(k-1)$ st minor locus. Assume that we  
1199 want to approximate the marginal distribution of the  $j$ th minor locus of an  $L$ -locus  
1200 model using a  $k$ -locus model,  $j < k < L$ . As for the case  $k = 2$  discussed above,  
1201 the approximation requires that the expected lag time between the establishment  
1202 of a mutation at a first locus and the establishment of a mutation at a  $j$ th locus be  
1203 matched. For the  $L$ -locus model, this waiting time is

$$\frac{1}{\Theta_l} \sum_{i=1}^j \frac{1}{L-i}.$$

1204 For a  $k$ -locus model with equal mutation rate  $\Theta_l^{(k)}$  at all loci, we thus obtain the  
1205 matching rule

$$\Theta_l^{(k)} = \Theta_l \frac{\sum_{i=1}^j \frac{1}{k-i}}{\sum_{i=1}^j \frac{1}{L-i}}$$

1206 for the approximation of the  $j$ th minor locus. For  $j = 1$ , this reproduces the  
 1207 matching rule for the background mutation rate  $\Theta_{bg}$ . In general, the value for  
 1208  $\Theta_l^k$  depends on  $j$ , but converges once  $L, k \gg j$ . Approximations by models  
 1209 with unequal locus mutation rates are also possible, but usually do not lead to  
 1210 a relevant improvement. In Fig 4, we use formulas from 3- and 4-locus models to  
 1211 approximate the marginal distributions of the 2nd and 3rd minor locus, respectively.  
 1212 In general, the approximations for all loci can be improved by using approximation  
 1213 models with more loci than required, i.e.  $k > j + 1$ . In Fig S.5, we show this for  
 1214 approximations of the major locus and the first three minor loci, all derived from a  
 1215 4-locus model.

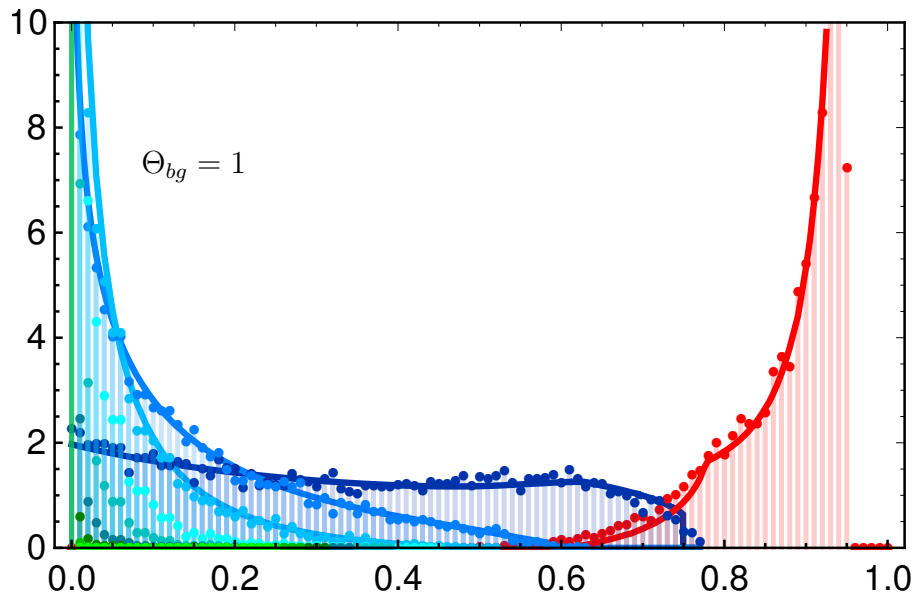


Figure S.5: **Approximating higher dimensional adaptive architectures for 10 loci**,  $\Theta_{bg} = 1$ . We approximate a 10 locus model with the theoretical predictions based on the four locus model for the major and the first, second and third minor locus. Compare Fig 4, where we use approximations based on the minimal number of loci needed.

## 1216 **A.5 Marginal distribution of a single locus**

1217 Figure S.6 shows the marginal distribution at a single focal locus for a trait with  $L$   
1218  $= 2$  to  $L=100$  loci in its basis. Since all loci are equal, the probability that the focal  
1219 locus ends up as the major locus is  $1/L$ . The red dots in the figure indicate the  
1220 part of the marginal distribution that corresponds to this case. With an increasing  
1221 number of redundant loci, the probability for each single locus to play a major  
1222 role in the adaptive process decreases. The marginal distribution of a fixed locus  
1223 therefore changes strongly with an increasing number of loci  $L$ . For large  $L$ , in  
1224 particular, it does not represent the key components of the adaptive architecture  
1225 on the level of the trait any more. This is in contrast to Fig 4, where marginal  
1226 distributions of the loci with the largest contributions to the adaptive response  
1227 are shown. For 2 loci, Fig S.6 also shows the analytical approximation for the  
1228 marginal distribution Eq (11). As long as the adaptive architecture is dominated  
1229 by only a few loci, the same 2-locus result can be used as an approximation for  
1230 the marginal distribution in models with more than two loci. This is shown in the  
1231 figure for  $\Theta_{bg} \leq 1$ . The figure also shows that the approximation fails for  $\Theta_{bg} \geq 10$   
1232 when adaptation is truly collective.

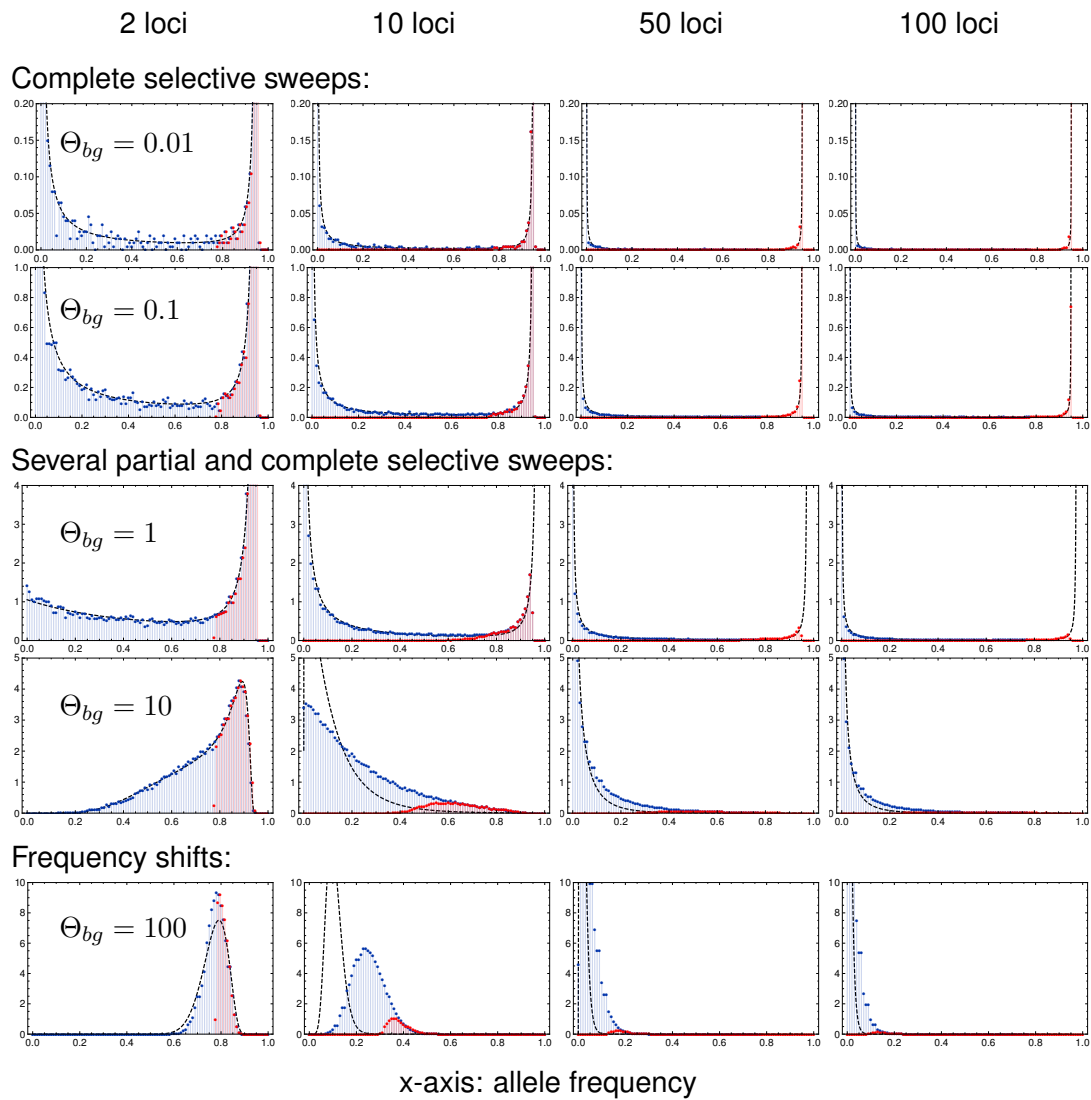


Figure S.6: **Marginal distribution at a single focal locus.** Simulation results for the marginal distribution at a single locus at the end of the adaptive phase are shown in blue. Red dots show the contribution of the major locus to this distribution (all cases, where the focal locus ends up as the major locus). Dashed lines show the analytical prediction for the 2-locus model, Eq (11). Parameters and further details as in Fig 4.

## 1233 **Acknowledgments**

1234 First, we want to thank Claus Vogl for his insightful comments and several fruitful  
1235 discussions. We also thank Matthias Maschek for his help concerning programming  
1236 and simulation setup. Finally, a special thank you goes to Montgomery Slatkin for  
1237 his hospitality in welcoming JH and IH to his lab at UC Berkeley, where this project  
1238 was started.

## 1239 **Data Archiving**

1240 We will provide a comprehensive *Mathematica* Inc. notebook, showing visualizations  
1241 of the derived analytical predictions. The simulation code will be made available  
1242 through the Dryad repository as a package.

1243 Höllinger I, Pennings PS, Hermisson J. Data from: Polygenic adaptation: From  
1244 sweeps to subtle frequency shifts. Dryad Digital Repository.

1245 <https://doi.org/10.5061/dryad.7n6vg10>

## 1246 **Funding**

1247 IH was funded by the Austrian Science Fund (FWF): DK W-1225-B20, Vienna  
1248 Graduate School of Population Genetics.

# Polygenic adaptation: From sweeps to subtle frequency shifts

## Mathematical Appendix

October 23, 2018

1 This Appendix describes the details of the mathematical model and methods  
2 used to derive the analytical results of the article. Section M.1 gives an outline  
3 of the model; section M.2 introduces the branching process method used for  
4 the early stochastic phase of polygenic adaptation; section M.3 describes the  
5 derivation of the joint frequency distribution at the end of the deterministic phase.

### 6 **M.1 Redundant trait model**

7 Consider a panmictic population of  $N_e$  haploids. Selection acts on a binary trait  
8  $Z$  (e.g. resistance) with just two states, a wildtype state  $Z_0$  (not resistant) and a  
9 mutant state  $Z_1$  (resistant). Without restriction, we can choose  $Z_0 = 0$  and  $Z_1 = 1$ .  
10 Malthusian (logarithmic) fitness is defined by the function

$$W(Z, t) = s(t)Z \tag{M.1}$$

11 where the time dependent coefficient  $s(t)$  defines the strength of directional selection.  
12 We assume that  $s(t) < 0$  for  $t < 0$ , but  $s(t) > 0$  for  $t > 0$ , such that the optimal  
13 trait value shifts from the wildtype state  $Z = 0$  to the mutant state  $Z = 1$  due to



14 some change in the environment at time  $t = 0$ . We also assume that selection is  
15 stronger than drift,  $|Ns(t)| \gg 1$  for almost all  $t$ , but is arbitrary otherwise.

16 We assume that  $Z$  is polygenic, with  $L$  biallelic loci (wildtype  $a_i$  and mutant  
17 allele  $A_i$ ,  $i = 1, \dots, L$ ) constituting its genetic basis. While genotype  $\mathbf{a} = (a_1, a_2, \dots, a_L)$   
18 produces the ancestral wildtype  $Z_0$ , all mutant genotypes are fully redundant and  
19 produce the mutant phenotype  $Z_1$ , independently of the number of mutations.  
20 New mutations from  $a_i$  to  $A_i$  occur at a rate  $\mu_i$  per generation, with  $\mu_i \ll |s(t)|$   
21 for almost all  $t$ . For the purpose of our model, back mutation from  $A_i$  to  $a_i$  can  
22 be ignored. The linkage map among loci is arbitrary – unless explicitly specified  
23 otherwise. Let  $p_i$  be the frequency of allele  $A_i$ , and let  $f_a$  be the frequency of the  
24 wildtype genotype  $\mathbf{a}$ . Then the mean fitness in the population is

$$\bar{W}(t) = s(t)\bar{Z}(t) = s(t)(f_a Z_0 + (1 - f_a)Z_1) \quad (\text{M.2a})$$

25 where  $\bar{Z}$  is the trait mean. Since  $W(Z_1, t) = s(t)Z_1$  is the marginal fitness of any  
26 mutant allele, the selection dynamics at the  $i$ th locus can be expressed as

$$\dot{p}_i = p_i(W(Z_1, t) - \bar{W}(t)) = s(t)p_i(Z_1 - \bar{Z}(t)). \quad (\text{M.2b})$$

27 Our redundancy assumption implies strong diminishing returns epistasis on the  
28 level of fitness: the fitness of genotypes with multiple mutations is the same as  
29 the one of single mutants. Eq (M.2b) shows that the epistatic effect of the genetic  
30 background on the dynamics at a particular locus is mediated by the trait mean  
31  $\bar{Z}(t)$  as single compound parameter. Allele frequencies at all loci change with the  
32 same (time and frequency-dependent) rate. We readily establish that

$$\frac{d}{dt} \left( \frac{p_i}{p_j} \right) = \frac{\dot{p}_i p_j - \dot{p}_j p_i}{p_j^2} = 0. \quad (\text{M.3})$$

33 Thus, the ratio of allele frequencies among loci does not change under selection.

34 Note that this holds for an arbitrary linkage map. We can conclude that any  
35 differences in (relative) allele frequencies are due to mutation and drift.

36 We are interested in the pattern of allele frequency changes across loci during  
37 the phase of rapid phenotypic adaptation. This phase starts with the onset of  
38 positive selection on derived alleles at time  $t = 0$ . It ends when mean fitness  
39  $\bar{W}(t)$  approaches its maximum  $s(t)Z_1$  and further selective change in the allele  
40 frequencies is strongly decelerated. Since  $(W(Z_1, t) - \bar{W}(t))/s(t) = (Z_1 - Z_0)f_a$ ,  
41 we can parametrize this end point by a condition  $f_a(t) = f_w$  on the frequency of  
42 the wildtype  $Z_0$  in the population. In our figures, we usually use  $f_w = 0.05$ . As  
43 initial state at time  $t = 0$ , we assume that the population adapts from a balance  
44 of mutation, selection, and drift. We thus allow for standing genetic variation  
45 (SGV) at all loci. If selection prior to  $t = 0$  is constant (which is what we generally  
46 assume in our computer simulations, see main text), SGV is given by the standard  
47 equilibrium distribution under mutation, selection, and drift, where we require that  
48  $a_i$  is the ancestral state at each locus. I.e., each allele frequency trajectory  $p_i(t)$ ,  
49 back in time, originates from the boundary  $p_i = 0$  rather than  $p_i = 1$  (see also  
50 Hermisson and Pennings (2005) for this concept). However, our analytical results  
51 do not require a static equilibrium and, for a general  $s(t) < 0$  for  $t < 0$ , the SGV  
52 reflects this non-equilibrium dynamics.

53 As described in the main text, we dissect the adaptive process into two phases.  
54 During an initial *stochastic phase* mutation, selection, and drift lead to the build-up  
55 of genetic variation, either from SGV or due to new mutation after time  $t = 0$ ,  
56 as long as allele frequencies  $p_i$  at all loci are still low. We will describe our  
57 approach to this phase in detail in the section on Yule processes below. Once  
58 allele frequencies are sufficiently large, genetic drift and recurrent new mutation  
59 play only a minor role relative to selection until we reach the end of the rapid  
60 adaptive phase. We thus enter a *deterministic phase* where the dynamics is then  
61 well approximated by Eq (M.2b).

## 62 Relaxed redundancy

63 To relax the stringent redundancy condition of our model, it is natural to assume  
64 that a single mutation is not sufficient to produce the full mutant phenotype  $Z_1 = 1$ ,  
65 but only a partial phenotype  $Z_q = q$  with  $0 < q < 1$ . This makes the marginal  
66 fitness of mutant alleles dependent on the genetic background. If genotypes with  
67 two or more mutations produce  $Z_1$ , we have

$$\dot{p}_i = (W_i(t) - \bar{W}(t))p_i = s(t)p_i \left( Z_1 - \bar{Z}(t) - (Z_1 - Z_q) \frac{f_i}{p_i} \right) \quad (\text{M.4})$$

68 where  $f_i$  is the frequency of the haplotype with a single mutation at locus  $i$ . Since  
69  $f_i/p_i$  depends on  $i$  (even in linkage equilibrium), the ratio of allele frequencies at  
70 different loci is no longer invariant and the key symmetry assumption (M.3) of the  
71 fully redundant model is violated. Note that redundancy is recovered for very low  
72 mutant frequencies, such that double mutants are rare ( $f_i \approx p_i$ ) and also late in  
73 the adaptation process, when most haplotypes carry at least one mutation and  
74  $f_i \rightarrow 0$ .

## 75 Diploids

76 We can generalize the redundant trait model to diploids as follows. For a general  
77 model, the dynamical equations in continuous time read

$$\dot{p}_i = (W_i(t) - \bar{W}(t))p_i \quad (\text{M.5})$$

78 where  $W_i(t)$  is the marginal fitness of allele  $A_i$  and  $\bar{W}(t)$  the mean fitness. All  
79 fitnesses may depend on the allele frequencies and on time. Using (M.3), we see  
80 that all mutant alleles  $A_i$  are redundant in the sense that they all feel the same  
81 selection pressure if and only if their marginal fitnesses are equal at all times,  
82  $W_i(t) = W_j(t), \forall i, j$ . (The same condition can also be derived from a discrete time

83 dynamics.) For haploids, equal marginal fitnesses, independently of the genetic  
84 composition of the population, enforces the fully redundant trait model described  
85 above. For diploids with dominance, the marginal fitness also depends on the  
86 allele frequency at the focal locus itself. An obvious solution to the condition  
87 of equal marginal fitnesses across loci is the case of complete dominance of  
88 the mutant allele. We can gain some more flexibility for the fitness scheme, if  
89 we assume that genotype frequencies are at Hardy-Weinberg equilibrium at all  
90 times. We can then distinguish three genotype classes: the wildtype without any  
91 mutations (normalized fitness 0), mutant individuals with one or more mutations  
92 on only a single haplotype (fitness  $s_1(t)$ ) and individuals with mutations on both  
93 haplotypes (fitness  $s_2(t)$ ). The marginal fitness of any mutant allele then is

$$W_i(t) = s_1(t)f_a + s_2(t)(1 - f_a), \quad (\text{M.6})$$

94 where  $f_a$  is the frequency of the ancestral haplotype without mutations. We thus  
95 require redundancy of mutations (only) within haplotypes. Note, however, that this  
96 fitness scheme implies a position effect, i.e., the fitness of the genotype does not  
97 only depend on the number of mutations at each locus, but also on the association  
98 of mutations to one or the other haplotype. If we assume linkage equilibrium in  
99 addition to Hardy-Weinberg proportions, a position effect can be avoided if we  
100 use the following fitness scheme

- 101 1. The ancestral genotype without any mutants has normalized fitness  $W(t) =$   
102 0,
- 103 2. any genotype with at least one homozygous mutant has fitness  $W(t) =$   
104  $s_2(t)$ ,
3. a genotype without a locus that is homozygous for the mutant, but with  $k$

loci that are heterozygous has fitness

$$W(t) = s_2(t) + 2^{1-k} \left( s_1(t) - s_2(t) \right).$$

105 Since  $2^{1-k}$  is the probability for any focal mutant allele to be on the same  
106 haplotype with all  $k - 1$  other mutant alleles, assuming linkage equilibrium,  
107 this fitness scheme leads to the same marginal fitness as Eq (M.6) above.

## 108 **M.2 Yule approximation**

109 We describe the dynamics of mutant types at the different loci during the stochastic  
110 phase by a *multi-type Yule pure birth process with immigration*. Our framework  
111 builds on established mathematical theory Joyce and Tavaré (1987); Durrett (2010)  
112 and a previous approach to describe the genealogy of a beneficial allele during a  
113 selective sweep in terms of a Yule process Etheridge et al. (2006); Hermisson and  
114 Pfaffelhuber (2008). Here, we extend this approach to the polygenic scenario.

115 Consider a mutation  $A_i$  that appears at some locus either prior to the environmental  
116 change (standing genetic variation) or after the change. This mutation is relevant  
117 for the joint distribution of mutant allele frequencies at the time of observation after  
118 the rapid adaptive phase if and only if descendants of this mutation still segregate  
119 in the population at this time. The idea of the Yule approach is to construct the  
120 genealogies of these mutant descendants at all loci forward in time. We start the  
121 process at some time  $t_0 \ll 0$  in the past before the first mutation with surviving  
122 descendants has originated. We assume that the frequency  $p_i$  of mutant alleles  
123 is low during the entire stochastic phase. Then, new mutations at locus  $i$  appear  
124 at rate  $\approx N\mu_i =: \Theta_i/2$  per generation, but only a fraction of those will survive  
125 deleterious selection prior to  $t = 0$  and genetic drift to establish in the population  
126 and to contribute to the adaptation of the trait. We denote this establishment  
127 probability as  $p_{\text{est}}(t)$ . If selection is constant and positive (as assumed in the main

128 text),  $s(t) = s_b > 0$ , we can approximate  $p_{\text{est}} \approx 2s_b$ . For general time-dependent  
129 selection,  $p_{\text{est}}(t)$  will depend on  $s(\tilde{t})$  with  $\tilde{t} \geq t$  Uecker and Hermisson (2011), and  
130 also on the mutations that were previously established at the same or at other  
131 loci. Crucially, however, since the marginal fitness of mutant copies at all loci is  
132 the same at any given time,  $p_{\text{est}}(t)$  does not depend on the locus. We only include  
133 mutants into our Yule process that successfully establish in the population, which  
134 are represented as “immortal lineages” in the Yule tree. We follow these lineages  
135 in continuous time. There are then two types of events:

136 1. First, new mutation creates new immortal lineages at rate

$$p_{\text{mut},i}(t) = \frac{\Theta_i}{2} p_{\text{est}}(t) \quad (\text{M.7})$$

137 independently at each locus. This event is called “immigration” in the mathematical  
138 literature Joyce and Tavaré (1987), but it corresponds to mutation in our  
139 model. (In a model with gene flow, where adaptation in a local deme occurs  
140 from immigration, new lines would be truly immigrants, see also Pennings  
141 and Hermisson (2006) for this analogy).

142 2. Second, existing immortal mutant alleles  $A_i$  can give birth to further immortal  
143 mutant copies, corresponding to a split of the immortal line in the Yule  
144 process. To derive the split rate  $p_{\text{split}}$ , imagine that we implement the evolutionary  
145 dynamics as a continuous-time Moran model, where individuals give birth  
146 (due to a binary split) at constant rate one per generation. In the corresponding  
147 Yule process, we only include this birth event if it leads to two immortal  
148 lineages. Obviously, the probability to “be immortal” for a newborn individual  
149 is the same as for a new mutation and given by  $p_{\text{est}}(t)$ . Conditioning on the  
150 fact that we only consider splits of immortal lineages and thus at least one of  
151 the offspring lineages must be immortal, we arrive at a split rate per immortal

152 lineage of

$$p_{\text{split}}(t) = \frac{p_{\text{est}}^2(t)}{p_{\text{est}}^2(t) + 2p_{\text{est}}(t)(1 - p_{\text{est}}(t))} = \frac{p_{\text{est}}(t)}{2 - p_{\text{est}}(t)} \approx \frac{p_{\text{est}}(t)}{2}, \quad (\text{M.8})$$

153 where the approximation in the last term assumes that  $p_{\text{est}}(t) \ll 1$ , which is  
154 usually the case unless selection is very strong.

155 The Yule process defines a continuous-time Markov process of a random variable  
156  $\mathbf{k} = (k_1, \dots, k_L)$ , where  $k_i \in \mathbb{N}_0$  is the number of immortal mutant lineages at the  
157  $i$ th locus. We are interested in the relative proportions in the number of lineages  
158  $k_i$  across loci after a sufficiently long time – assuming that the distribution of these  
159 proportions reaches a limit by the end of the stochastic phase. We can generate  
160 this distribution from the transition probabilities among Yule states (the embedded  
161 jump-chain of the continuous-time process). If there are currently  $(k_1, \dots, k_L)$   
162 lineages at the  $L$  loci, the probability that the next event is either a birth event  
163 (split) or a new mutation (immigration) at locus  $i$  is

$$\begin{aligned} \Pr[(k_1, \dots, k_L) \rightarrow (k_1, \dots, k_i + 1, \dots, k_L)] \\ = \frac{k_i p_{\text{split}} + p_{\text{mut},i}}{\sum_{j=1}^L (k_j p_{\text{split}} + p_{\text{mut},j})} = \frac{k_i + \Theta_i}{\sum_{j=1}^L (k_j + \Theta_j)}. \end{aligned} \quad (\text{M.9})$$

164 Crucially, these transition probabilities are constant in time and independent of the  
165 establishment probability  $p_{\text{est}}(t)$ . As a consequence, they are also independent of  
166 the mutant fitness, which only affects the speed of the Yule process (via  $p_{\text{est}}$ ), but  
167 not its sequence of events.

168 We start the process with no mutants and stop it whenever the number of  
169 mutants at one of the loci (e.g. locus 1) reaches some number  $k_1 = n$ . We are  
170 interested in the distribution of the number of mutants  $k_i$  at the other loci at this  
171 time, respectively their ratios  $k_i/n$  (remember that we already know that these  
172 ratios stay invariant during the deterministic phase of the adaptation process).

173 We can prove the following

174 **Theorem 1** In the limit of  $n \rightarrow \infty$ , the joint distribution of ratios  $x_i = k_i/n$  of  
 175 immortal mutant lineages across loci converges to the *inverted Dirichlet distribution*,

$$P_{\text{inDir}}[\{x_i\}_{i \geq 2} | \Theta] = \frac{1}{B[\Theta]} \prod_{j=2}^L x_j^{\Theta_j - 1} \left(1 + \sum_{j=2}^L x_j\right)^{-\sum_{j=1}^L \Theta_j} \quad (\text{M.10})$$

176 where the vector  $\Theta = (\Theta_1, \dots, \Theta_L)$  summarizes the mutation rates and  $B[\Theta]$  is the  
 177 multivariate Beta function, which can be expressed in terms of Gamma functions  
 178 as

$$B[\Theta] = \frac{\prod_{i=1}^L \Gamma(\Theta_i)}{\Gamma(\sum_{i=1}^L \Theta_i)}. \quad (\text{M.11})$$

179 **Proof** We proceed in three steps.

180 **Step 1** Assume that we stop the process when the first locus reaches  $n >$   
 181 0 lineages. We derive the probability that the process at this time is in state  
 182  $(n, k_2, \dots, k_L)$  as follows. We need  $n + k_2 + \dots + k_L$  events (new mutations or  
 183 splits) to generate all mutant individuals. The last event must occur at the first  
 184 locus. All other events can occur in arbitrary order at the  $L$  loci. The probability of  
 185 each realization (each order of events at the loci) is given by the corresponding  
 186 product of transition probabilities (M.9). The key insight is that all realizations  
 187 have the same probability. Indeed, the denominator of (M.9) does not depend on  
 188 the locus where the next event occurs. Different realizations then only correspond  
 189 to permutations in the factors  $k_i + \Theta_i$  in the numerator of the product of transition  
 190 probabilities. We can directly write down the probability for the state as

$$\Pr[\{k_i\}_{i \geq 2} | n, \Theta] = \binom{n-1+k_2+\dots+k_L}{n-1, k_2, \dots, k_L} \frac{(\Theta_1)_{(n)} \prod_{j=2}^L (\Theta_j)_{(k_j)}}{(\Theta_1 + \dots + \Theta_L)_{(n+k_2+\dots+k_L)}}, \quad (\text{M.12})$$

where

$$\Theta_{(k)} := \Theta(\Theta + 1) \dots (\Theta + k - 1)$$



191 is the Pochhammer function. The leading multinomial coefficient counts the number  
 192 of all permutations and the ratio of Pochhammer functions is the probability of  
 193 each realization.

194 **Step 2** We can rewrite (M.12) as a *Dirichlet-negative-multinomial* compound  
 195 distribution, defined as

$$\int_0^1 \cdots \int_0^1 \binom{n-1+k_2+\cdots+k_L}{n-1, k_2, \dots, k_L} \prod_{i=2}^L y_i^{k_i} \left(1 - \sum_{i=2}^L y_i\right)^n f(\{y_i\}_{i \geq 2} | \Theta) dy_2 \cdots dy_L, \quad (\text{M.13})$$

196 where

$$f(\{y_i\}_{i \geq 2} | \Theta) = \frac{1}{B[\Theta]} \prod_{i=2}^L y_i^{\Theta_i-1} \left(1 - \sum_{i=2}^L y_i\right)^{\Theta_1-1}$$

197 is the  $(L-1)$ -dimensional Dirichlet distribution for a  $L$ -dimensional probability  
 198 vector  $(y_1, \dots, y_L)$  with constraint  $y_1 = 1 - \sum_{i \geq 2} y_i$ . This is best shown in the  
 199 reverse direction, i.e., by deriving (M.12) from (M.13). To see this, note that

$$\int_0^1 \cdots \int_0^1 \prod_{i=2}^L y_i^{\Theta_i+k_i-1} \left(1 - \sum_{i=2}^L y_i\right)^{\Theta_1+n-1} dy_2 \cdots dy_L = \frac{\Gamma(\Theta_1+n) \prod_{i=2}^L \Gamma(\Theta_i+k_i)}{\Gamma(\Theta_1+n + \sum_{i=2}^L (\Theta_i+k_i))}$$

because the integrand in this expression is just a Dirichlet density with shifted  
 values of  $\Theta_i \rightarrow \Theta_i + k_i$  and the right hand side is the corresponding normalization  
 factor. Then using

$$\frac{\Gamma(\sum_{i=1}^L \Theta_i) \Gamma(\Theta_1+n) \prod_{i=2}^L \Gamma(\Theta_i+k_i)}{\prod_{i=1}^L \Gamma(\Theta_i) \Gamma(\Theta_1+n + \sum_{i=2}^L (\Theta_i+k_i))} = \frac{(\Theta_1)_{(n)} \prod_{j=2}^L (\Theta_j)_{(k_j)}}{(\Theta_1 + \cdots + \Theta_L)_{(n+k_2+\cdots+k_L)}}$$

200 reduces (M.13) to (M.12).

201 The compound distribution Eq (M.13) can be interpreted as follows: If a random  
 202 experiment can have a finite number of outcomes (here: mutant lineages at one of

203  $L$  loci), the negative multinomial distribution describes the probability to observe  
204 each of these events  $k_i$  times if we repeat the experiment until a focal event  
205 (here: new mutant lineage at the first locus) has occurred  $n$  times. While the  
206 negative multinomial distribution assumes that all outcomes occur with a fixed  
207 probability  $y_i$ , this probability is itself drawn from a Dirichlet distribution in the  
208 Dirichlet-negative-multinomial compound distribution. In the present context, the  
209 main advantage of (M.13) over (M.12) is that we can easily perform the limit  
210  $n \rightarrow \infty$  in this form.

211 **Step 3** For large  $n \rightarrow \infty$ , the values of  $k_i/n$ ,  $i \geq 2$ , of the negative multinomial  
212 distribution can be replaced by their expectations,

$$x_i := \mathbb{E} \left[ \frac{k_i}{n} \right] = \frac{y_i}{1 - \sum_{j=2}^L y_j} \Leftrightarrow y_i = \frac{x_i}{1 + \sum_{j=2}^L x_j}.$$

213 We can then transform the density (M.10) from variables  $y_i$  to the  $x_i$  (representing  
214 the relative mutant frequencies). The entries of the Jacobian matrix (for  $2 \leq i, j \leq$   
215  $L$ ) are

$$\mathbf{J}_{ij} = \frac{\partial y_i}{\partial x_j} = \frac{\delta_{i,j}(1 + \sum_{k=2}^L x_k) - x_i}{(1 + \sum_{k=2}^L x_k)^2}.$$

216 Since this is the sum of an identity matrix (times a factor) and a matrix with  
217 identical columns we can easily derive the eigenvalues and thus the determinant,

$$\text{Det}[\mathbf{J}] = \frac{1}{(1 + \sum_{k=2}^L x_k)^L}.$$

218 Applying this transformation to (M.13), we obtain (M.10).

### 219 **Remarks**

1. For two loci, the Dirichlet-negative-multinomial distribution (M.13) reduces

to a *Beta-negative-binomial* distribution

$$P_{\beta NB}[k|n] = \int_0^1 \binom{n+k-1}{k} y^k (1-y)^n \frac{\Gamma(\Theta_1 + \Theta_2)}{\Gamma(\Theta_1)\Gamma(\Theta_2)} y^{\Theta_2-1} (1-y)^{\Theta_1-1} dy$$

220 and the inverted Dirichlet distribution (M.10) simplifies to a so-called  *$\beta$ -prime*  
 221 distribution,

$$P_{\beta'}(x) = \frac{\Gamma(\Theta_1 + \Theta_2)}{\Gamma(\Theta_1)\Gamma(\Theta_2)} x^{\Theta_2-1} (1+x)^{-\Theta_1-\Theta_2}. \quad (\text{M.14})$$

222 If we measure the ratio  $x$  always relative to the locus with the higher frequency,  
 223 we obtain a conditioned distribution that is truncated at  $x = 1$ . For equal  
 224 locus mutation rates  $\Theta_1 = \Theta_2 = \Theta_l$ , in particular,

$$P_{\beta'}[x|\Theta_l] = \frac{2\Gamma(2\Theta_l)}{(\Gamma(\Theta_l))^2} x^{\Theta_l-1} (1+x)^{-2\Theta_l}. \quad (\text{M.15})$$

225 with expectation

$$\mathbf{E}[x] = \int_0^1 x P_{\beta'}[x|\Theta_l] dx = \frac{2\Gamma(2\Theta_l) {}_2F_1[2\Theta_l, 1 + \Theta_l, 2 + \Theta_l, -1]}{(1 + \Theta_l)(\Gamma(\Theta_l))^2}, \quad (\text{M.16})$$

226 where  ${}_2F_1$  is the hypergeometric function.

227 2. The process described here is a variant of the *Polya urn* and *Hoppe urn*  
 228 processes that are well-known in the mathematical literature and have been  
 229 used to describe coalescent processes forward in time Joyce and Tavaré  
 230 (1987); Durrett (2010).

231 3. Our result (M.10) can also be seen as multi-locus version of Wright's formula  
 232 for the stationary distribution of the Wright-Fisher diffusion Wright (1931).  
 233 For  $L$  neutral alleles at a single locus, and if the mutation rates  $\Theta_i$  depend  
 234 only on the target allele (house-of-cards condition), this is a Dirichlet distribution.  
 235 Here, we see that an analogous result holds for a distribution of equivalent  
 236 (mutually redundant) alleles across  $L$  loci. Although alleles at different

237 loci cannot mutate into each other and are never identical by descent, it  
238 turns out that the genealogy in both models can be described by a Yule  
239 process with immigration. In contrast to the single-locus case, we obtain an  
240 *inverted* Dirichlet distribution for multiple loci. This difference results from  
241 a different stopping condition for the Yule process. For a single locus, the  
242 population size sets an upper bound for the total number of copies across  
243 all alleles. If we stop the process for a given total number  $n_{\text{tot}}$  of lines, we  
244 obtain the classical Dirichlet distribution in the limit  $n_{\text{tot}} \rightarrow \infty$ . In contrast,  
245 the population size defines a bound for mutants of a only single type in the  
246 multi-locus case, which is reflected by our choice of the stopping condition.  
247 This choice is appropriate unless all loci are tightly linked, as we will see  
248 below.

249 4. In our model, we did not distinguish different mutational origins of mutant  
250 alleles at the same locus. It is, in principle, possible to do so. For any  
251 single locus, the process *conditioned on* reaching some number of mutants  
252  $k_i$  at this locus  $i$  is entirely independent of the process at the other loci. The  
253 joint distribution of different mutational origins at this locus is therefore given  
254 by the Ewens sampling formula, as described in the theory of soft selective  
255 sweeps (Pennings and Hermisson (2006); Hermisson and Pennings (2017)).

### 256 **M.3 Allele frequency distributions**

257 Eq (M.10) predicts the distribution of allele frequency ratios  $x_i$  at the end of  
258 the stochastic phase of the adaptive process. Typically, the Yule process will  
259 approach convergence for  $n \gtrsim 100$ . In a large population, this still corresponds  
260 to a small allele frequency. However, since the allele frequency ratios remain  
261 constant also during the deterministic phase, we can use the Yule process result  
262 to derive the distribution of mutant allele frequencies also at a later stage, when  
263 (partial or complete) phenotypic adaptation has been achieved. As above, we

264 characterize the time of observation via the frequency of the ancestral phenotypes  
 265  $f_w$  that is still found in the population. We treat the case of full adaptation,  $f_w = 0$ ,  
 266 before we turn to the case of a general  $f_w$ .

267 **Complete phenotypic adaptation,  $f_w = 0$**

268 If selection is very strong, complete fixation of the mutant phenotype may be  
 269 rapidly achieved. For any non-zero level of recombination among loci,  $f_w = 0$   
 270 requires, in our model, that there is (at least) a single locus where the mutant  
 271 allele has reached fixation. In the following, we will call the locus with the largest  
 272 mutant frequency the *major locus* and all other loci *minor loci*. We are interested  
 273 in the joint distribution of allele frequencies when the major locus has reached  
 274 fixation. From (M.10), we can derive the probability that the first locus ends up  
 275 being the major locus as

$$P_{1>}^{(\Theta)} = \int_0^1 \dots \int_0^1 P_{\text{inDir}}[\{x_i\}_{i \geq 2} | \Theta] dx_2 \dots dx_L. \quad (\text{M.17})$$

276 Since allele frequencies  $p_i$  equal allele frequency ratios  $x_i$  relative to the major  
 277 locus in this case, the joint distribution at all minor loci,  $\{p_i\}_{i \geq 2}$ ,  $0 \leq p_i \leq 1$ ,  
 278 conditioned on fixation of the mutant allele at the first locus, follows as  $P_{\text{inDir}}[\{p_i\}_{i \geq 2} | \Theta] / P_{1>}[\Theta]$ .  
 279 The joint allele frequency distribution for all loci at  $f_w = 0$  results as product of a  
 280 Dirac point measure at the major locus and truncated inverted Dirichlet densities  
 281 at the minor loci. Summing over all possible loci as major locus we obtain

$$P_0[\{p_i\}_{i \geq 1} | \Theta] = \sum_{k=1}^L \left( \frac{\delta_{p_k-1}}{B[\Theta]} \prod_{j \neq k} p_j^{\Theta_j-1} \left( 1 + \sum_{j \neq k} p_j \right)^{-\sum_{j=1}^L \Theta_j} \right), \quad (\text{M.18})$$

282 where the Dirac  $\delta$  constrains the distribution to the boundary faces  $p_k = 1$  of the  
 283  $L$ -dimensional hypercube  $[0, 1]^L$  of allele frequencies. Note that this formula is  
 284 independent of linkage patterns as long as loci can recombine at all and are not  
 285 completely linked (see below for this case).

286 **Incomplete phenotypic adaptation,  $f_w > 0$ , linkage equilibrium**

287 While the distribution of allele frequency *ratios*  $x_i$ , Eq (M.10), holds for any time  
 288 of observation during the adaptive process (once the Yule process has reached  
 289 convergence), the corresponding distribution (M.18) for the *absolute* allele frequencies  
 290  $p_i$  holds only for complete phenotypic adaptation,  $f_w = 0$ . To derive this distribution  
 291 for arbitrary  $f_w \geq 0$ , we need to translate the stopping condition for the ancestral  
 292 phenotype to a condition on the  $p_i$ . For  $f_w = 0$ , this just leads to the condition  $p_k =$   
 293 1 for the major locus, constraining the distribution (M.18) to the boundary faces  
 294 of the allele frequency hypercube. Importantly, this constraint is independent of  
 295 linkage. For  $f_w > 0$ , in contrast, any constraint on the distribution of the  $p_i$  due to  
 296 the stopping condition will necessarily also depend on the linkage disequilibria.  
 297 For further analytical progress we now assume that recombination is sufficiently  
 298 strong that linkage disequilibria can be ignored. We then obtain

$$\prod_{j=1}^L (1 - p_j) = f_w \quad (\text{M.19})$$

299 and the joint allele frequency distribution is given by the following Theorem, which  
 300 is our main analytical result.

301 **Theorem 2** If the adaptive process is stopped at a frequency  $f_w$  of the ancestral  
 302 phenotype in the population, and assuming linkage equilibrium among loci, the  
 303 joint distribution of mutant frequencies on the  $L$ -dimensional hypercube is

$$P_{f_w}[\{p_i\}_{i \geq 1} | \Theta] = \frac{\delta_{\prod_{j=1}^L (1-p_j) - f_w}}{B[\Theta]} \prod_{i=1}^L p_i^{\Theta_i - 1} \left( \sum_{j=1}^L p_j \right)^{-\sum_{j=1}^L \Theta_j} \left( \sum_{j=1}^L \frac{f_w p_j}{1 - p_j} \right), \quad (\text{M.20})$$

304 where the  $\delta$ -function restricts the support of  $P_{f_w}[\{p_i\}_{i \geq 1} | \Theta]$  to the  $(L-1)$ -dimensional  
 305 submanifold  $\prod_{j=1}^L (1 - p_j) = f_w$ .

306 **Proof** We can rewrite (M.19) as condition on the frequency  $p_1$  at the first locus,

$$p_1 = 1 - \frac{f_w}{\prod_{j=2}^L (1 - p_j)} \quad (\text{M.21})$$

307 to obtain the transformation from frequency ratios  $x_i$  to absolute allele frequencies

308  $p_i, i \geq 2,$

$$x_i = \frac{p_i}{p_1} = \frac{p_i \prod_{j=2}^L (1 - p_j)}{\prod_{j=2}^L (1 - p_j) - f_w}. \quad (\text{M.22})$$

309 The corresponding Jacobian matrix reads ( $2 \leq i, j \leq L$ )

$$\begin{aligned} \tilde{\mathbf{J}}_{ij} &= \frac{\partial x_i}{\partial p_j} = \frac{p_i}{1 - p_j} \frac{f_w \prod_{k=2}^L (1 - p_k)}{(\prod_{k=2}^L (1 - p_k) - f_w)^2} + \delta_{i,j} \frac{\prod_{k=2}^L (1 - p_k)}{\prod_{k=2}^L (1 - p_k) - f_w} \\ &= \frac{p_i}{1 - p_j} \frac{1 - p_1}{p_1^2} + \frac{\delta_{i,j}}{p_1}. \end{aligned}$$

Thus

$$\tilde{\mathbf{J}} = \frac{1 - p_1}{p_1^2} \mathbf{Q} + \frac{1}{p_1} \mathbf{I},$$

310 where  $\mathbf{I}$  is the identity matrix and  $\mathbf{Q}_{i,j} = p_i/(1 - p_j)$ . Since  $\mathbf{Q}$  has the eigenvalue

311  $\sum_j p_j/(1 - p_j)$  and a  $(L - 2)$ -fold eigenvalue 0, we obtain the spectrum of  $\tilde{\mathbf{J}}$  and

312 thus the determinant

$$\text{Det}[\tilde{\mathbf{J}}] = p_1^{1-L} \left( \sum_{j=1}^L \frac{p_j(1 - p_1)}{(1 - p_j)p_1} \right). \quad (\text{M.23})$$

From (M.10), we then obtain the joint distribution of locus frequencies  $p_2, \dots, p_L$  at the stopping condition (M.21) as

$$\begin{aligned} \mathbf{P}_{f_w}[\{p_i\}_{i \geq 2} | \Theta] &= \frac{\text{Det}[\tilde{\mathbf{J}}]}{B[\Theta]} \prod_{i=2}^L \left( \frac{p_i}{p_1} \right)^{\Theta_i - 1} \left( 1 + \sum_{j=2}^L \frac{p_j}{p_1} \right)^{-\sum_{j=1}^L \Theta_j} \\ &= \frac{1}{B[\Theta]} \prod_{i=1}^L p_i^{\Theta_i - 1} \left( \sum_{j=1}^L p_j \right)^{-\sum_{j=1}^L \Theta_j} \left( \sum_{j=1}^L \frac{p_j(1 - p_1)}{1 - p_j} \right) \quad (\text{M.24}) \end{aligned}$$

313 where the dependence on  $f_w$  is implicit in  $p_1 = p_1(f_w)$ , as given in (M.21). The  
 314 joint distribution over all  $L$  loci follows as

$$\mathbf{P}_{f_w}[\{p_i\}_{i \geq 1} | \Theta] = \delta_{p_1 - 1 + f_w / \prod_{j=2}^L (1 - p_j)} \mathbf{P}_{f_w}[\{p_i\}_{i \geq 2} | \Theta]. \quad (\text{M.25})$$

Note that we do not assume that the first locus is the major locus in (M.25).

Finally, the symmetrical form (M.20) results from the relation

$$\delta_{g(x)-c} = \frac{\delta_{x-x_c}}{|g'(x)|_{x_c}} \quad ; \quad g(x_c) = c$$

315 for the Dirac  $\delta$ -function.

## 316 **Remarks**

317 1. To obtain marginal distributions for single loci we generally need to perform  
 318 a  $(L - 2)$ -dimensional integral (after resolving the  $\delta$ -function). Details for  
 319 specific cases used in the main part of the article are provided in the Mathematica  
 320 notebook. For two loci, simple explicit formulas for marginal distributions can  
 321 be derived. E.g., the marginal distribution at the first locus reads

$$\mathbf{P}_{f_w}[p_1 | \Theta_1, \Theta_2] = \frac{p_1^{\Theta_1 - 1} (1 - p_1 - f_w)^{\Theta_2 - 1} (1 - p_1)^{\Theta_1 + 1}}{B[\Theta_1, \Theta_2] (1 - p_1^2 - f_w)^{\Theta_1 + \Theta_2}} \left( 1 - \frac{f_w (1 - 2p_1)}{(1 - p_1)^2} \right) \quad (\text{M.26})$$

322 for  $0 \leq p_1 \leq f_w$ . The distribution has singularities at  $p_1 = 0$  for  $\Theta_1 < 1$  and  
 323 at  $p_1 = 1 - f_w$  for  $\Theta_2 < 1$ . The distributions  $\mathbf{P}_{f_w}^+[p | \Theta_1, \Theta_2]$  at the major locus  
 324 and  $\mathbf{P}_{f_w}^- [p | \Theta_1, \Theta_2]$  at the minor locus (which can either be locus 1 or locus 2)  
 325 follow as

$$\mathbf{P}_{f_w}^\pm [p | \Theta_1, \Theta_2] = (\mathbf{P}_{f_w}[p | \Theta_1, \Theta_2] + \mathbf{P}_{f_w}[p | \Theta_2, \Theta_1]) H_{\pm(p - 1 + \sqrt{f_w})} \quad (\text{M.27})$$

326 where  $H(x)$  is the Heaviside function with  $H_x = 1$  for  $x \geq 0$  and  $H_x = 0$   
 327 else. Finally, the *conditioned* distributions  $\mathbf{P}_{f_w}^{1 \geq} [p_1 | \Theta_1, \Theta_2]$  at the first locus if



328

this locus is the major/minor locus are

$$P_{f_w}^{1>}[p_1|\Theta_1, \Theta_2] = \frac{P_{f_w}[p_1|\Theta_1, \Theta_2]}{P_{1>}^{(\Theta_1, \Theta_2)}} H_{p_1-1+\sqrt{f_w}}, \quad (\text{M.28a})$$

$$P_{f_w}^{1<}[p_1|\Theta_1, \Theta_2] = \frac{P_{f_w}[p_1|\Theta_1, \Theta_2]}{1 - P_{1>}^{(\Theta_1, \Theta_2)}} H_{-(p_1-1+\sqrt{f_w})}, \quad (\text{M.28b})$$

329 where  $P_{1>}^{(\Theta_1, \Theta_2)}$ , defined in Eq (M.17), evaluates to a Hypergeometric function  
 330 for general  $\Theta_1 \neq \Theta_2$ , but reduces to 1/2 for  $\Theta_1 = \Theta_2$ .

2. The marginal distribution for  $p_k$  has a singularity at  $p_k = 0$  for  $\Theta_k < 1$  and a singularity at  $p_k = 1 - f_w$  for  $\sum_{j \neq k}^L \Theta_j < 1$ . To see this, consider the marginal distribution of  $p_L$ , which is obtained from Eq. (M.25) after integration over  $p_1, \dots, p_{L-1}$ . Dropping non-singular terms (such as the sums in Eq M.24), and defining

$$q_k = \frac{\prod_{j=k+1}^L (1 - p_j) - f_w}{\prod_{j=k+1}^L (1 - p_j)}$$

the singular part can be written as

$$\begin{aligned} P_{f_w}[p_L|\Theta] &\sim \int_0^1 \int_0^1 \dots \int_0^1 \delta_{p_1-q_1} \prod_{i=1}^L p_i^{\Theta_i-1} dp_1 \dots dp_{L-1} \\ &= \int_0^{q_{L-1}} \int_0^{q_{L-2}} \dots \int_0^{q_2} q_1^{\Theta_1-1} \prod_{i=2}^L p_i^{\Theta_i-1} dp_2 \dots dp_{L-1}, \end{aligned}$$

after performing the  $p_1$  integral. The upper integral limits  $q_k$  account for the constraint  $q_1 > 0$ . Substituting

$$\tilde{p}_2 := \frac{p_2}{q_2} \quad \Rightarrow \quad dp_2 = q_2 d\tilde{p}_2$$

and using that  $q_1 = q_2(1 - \tilde{p}_2)/(1 - \tilde{p}_2 q_2)$  we obtain

$$\begin{aligned} P_{f_w}[p_L|\Theta] &\sim \int_0^{q_{L-1}} \dots \int_0^{q_3} \int_0^1 q_1^{\Theta_1-1} q_2^{\Theta_2} \tilde{p}_2^{\Theta_2-1} \prod_{i=3}^L p_i^{\Theta_i-1} d\tilde{p}_2 dp_3 \dots dp_{L-1} \\ &= \int_0^{q_{L-1}} \dots \int_0^{q_3} q_2^{\Theta_1+\Theta_2-1} \int_0^1 \left( \frac{1 - \tilde{p}_2}{1 - \tilde{p}_2 q_2} \right)^{\Theta_1-1} \tilde{p}_2^{\Theta_2-1} d\tilde{p}_2 \prod_{i=3}^L p_i^{\Theta_i-1} dp_3 \dots dp_{L-1}. \end{aligned}$$

331 Since the  $\tilde{p}_2$  integral is bounded by  $1/\Theta_2$  from below and by  $1/\Theta_2 + 1/\Theta_1$  from  
332 above for all  $0 \leq q_2 \leq 1$ , it does not contribute to a singularity in  $P_{f_w}[p_L|\Theta]$ .

333 For the singular part, we thus have

$$P_{f_w}[p_L|\Theta] \sim \int_0^{q_{L-1}} \dots \int_0^{q_3} q_2^{\Theta_1+\Theta_2-1} \prod_{i=3}^L p_i^{\Theta_i-1} dp_3 \dots dp_{L-1}.$$

334 Iterating the substitution procedure for variables  $p_3$  to  $p_{L-1}$ , we arrive at

$$P_{f_w}[p_L|\Theta] \sim q_{L-1}^{\sum_{j=1}^{L-1} \Theta_j-1} p_L^{\Theta_L-1} = \left( \frac{1 - f_w - p_L}{1 - p_L} \right)^{\sum_{j=1}^{L-1} \Theta_j-1} p_L^{\Theta_L-1},$$

335 demonstrating the singular behavior for  $p_L \rightarrow 0$  and for  $p_L \rightarrow 1 - f_w$ . Since  
336 the labeling of loci is arbitrary, the assertion follows for all loci.

### 337 **Incomplete phenotypic adaptation, $f_w > 0$ , tight linkage**

338 Even if all loci are completely linked, the joint distribution of allele frequency *ratios*  
339 is still given by (M.10). However, the transformation to absolute allele frequencies  
340 at the stopping condition  $f_w \neq 0$  depends on linkage. Because all mutant alleles  
341 are rare during the stochastic phase, we can ignore haplotypes with more than  
342 a single mutant during this time. Since we ignore new mutations during the  
343 deterministic phase, mutant alleles stay in maximal linkage disequilibrium in the  
344 absence of recombination. We thus have

$$\sum_{j=1}^L p_j = 1 - f_w \quad \Rightarrow \quad x_i = \frac{p_i}{p_1} = \frac{p_i}{1 - f_w - \sum_{j=2}^L p_j}$$

with corresponding Jacobian

$$\mathbf{J}_{ij} = \frac{\partial x_i}{\partial p_j} = \frac{p_i + \delta_{i,j} p_1}{p_1^2} \quad ; \quad \text{Det}[\mathbf{J}] = \frac{1 - f_w}{p_1^L}.$$

Using this transformation on (M.10), the joint distribution of mutant frequencies reads

$$\mathbf{P}_{f_w, \text{tl}}[\{p_i\}_{i \geq 1} | \Theta] = \frac{\delta_{\sum_{i=1}^L p_i - 1 + f_w}}{B[\Theta] (1 - f_w)^{L-1}} \prod_{i=1}^L \left( \frac{p_i}{1 - f_w} \right)^{\Theta_i - 1}. \quad (\text{M.29})$$

345 Evidently, this is just the Dirichlet distribution on the cube  $[0, 1 - f_w]^L$ . This is  
 346 expected since the problem reduces to a single-locus,  $L$ -alleles problem for tight  
 347 linkage. The marginal distributions can be derived for an arbitrary number of loci  
 348 and are given by transformed  $\beta$ -distributions,

$$\mathbf{P}_{f_w, \text{tl}}[p_k | \Theta] = \frac{(1 - f_w)^{-1}}{B[\Theta]} \left( \frac{p_k}{1 - f_w} \right)^{\Theta_k - 1} \left( 1 - \frac{p_k}{1 - f_w} \right)^{(\sum_{j \neq k} \Theta_j) - 1}, \quad (\text{M.30})$$

349 with singularities at the boundaries  $p_k = 0$  for  $\Theta_k < 1$  and at  $p_k = 1 - f_w$   
 350 for  $\sum_{j \neq k} \Theta_j < 1$  as in the linkage equilibrium case. For two tightly linked loci,  
 351 the major locus must have frequency  $p > (1 - f_w)/2$ . The distribution at the  
 352 major/minor locus therefore reads

$$\mathbf{P}_{f_w, \text{tl}}^{\pm}[p | \Theta_1, \Theta_2] = (\mathbf{P}_{f_w, \text{tl}}[p | \Theta_1, \Theta_2] + \mathbf{P}_{f_w, \text{tl}}[p | \Theta_2, \Theta_1]) H_{\pm(p - (1 - f_w)/2)} \quad (\text{M.31})$$

353 and conditioned distributions follow as in (M.28).

## 354 References

355 Durrett, R. (2010). *Probability: theory and examples*. Cambridge university press.

- 356 Etheridge, A., Pfaffelhuber, P., Wakolbinger, A., et al. (2006). An approximate sampling  
357 formula under genetic hitchhiking. *The Annals of Applied Probability*, 16(2):685–729.
- 358 Hermisson, J. and Pennings, P. S. (2005). Soft sweeps: molecular population genetics of  
359 adaptation from standing genetic variation. *Genetics*, 169(4):2335–2352.
- 360 Hermisson, J. and Pennings, P. S. (2017). Soft sweeps and beyond: understanding the  
361 patterns and probabilities of selection footprints under rapid adaptation. *Methods in*  
362 *Ecology and Evolution*, 8(6):700–716.
- 363 Hermisson, J. and Pfaffelhuber, P. (2008). The pattern of genetic hitchhiking under  
364 recurrent mutation. *Electronic Journal of Probability*, 13:2069–2106.
- 365 Joyce, P. and Tavaré, S. (1987). Cycles, permutations and the structure of the yule  
366 process with immigration. *Stochastic processes and their applications*, 25:309–314.
- 367 Pennings, P. and Hermisson, J. (2006). Soft sweeps ii—molecular population genetics  
368 of adaptation from recurrent mutation or migration. *Molecular biology and evolution*,  
369 23(5):1076–1084.
- 370 Uecker, H. and Hermisson, J. (2011). On the fixation process of a beneficial mutation in  
371 a variable environment. *Genetics*, pages genetics–110.
- 372 Wright, S. (1931). Evolution in mendelian populations. *Genetics*, 16(2):97.